

# An internal sensory model allows for balance control using muscle spindle exafferent acceleration feedback

Eric Maris\*, #

*\*Donders Institute for Brain, Cognition, and Behaviour, Radboud University, P.O. Box 9104 HE Nijmegen*

#

Corresponding Author:

Eric Maris

e-mail: e.maris@donders.ru.nl

tel: +31243612651

The total number of words of the manuscript, including entire text from title page to figure legends:

The number of words of the abstract:

The number of figures: **4**

The number of tables: 0

## Abstract

All motor tasks with an approximately linear mechanical system (e.g., a freely standing person, a rider on a bicycle) allows for optimal control actions that are a simple linear combination of full state sensory feedback. When the sensory feedback is not full state (i.e., does not contain position and velocity information about all joints), optimal control for these systems is based on an internal dynamical system that estimates the states, and that can be implemented as a recurrent neural network (RNN) in the central nervous system (CNS). It uses a sensory model to update the state estimates with the available (non-full state) sensory feedback. The weights of this RNN are fully specified by results from optimal feedback control. This is highly relevant for all sensory systems that do not provide full state feedback, and especially for muscle spindle primary afferents under well-coordinated fusimotor and skeletomotor control because, under this condition, their firing rates scale with the exafferent joint acceleration component. A sensory model exists for this exafferent acceleration component, and this can be used by the CNS to estimate the states. As a proof of the viability of this mechanism, I demonstrate that it balances a standing body and a rider-bicycle combination using realistic parameter values and with forcing torques that are feasible for humans.

### Keywords

*Internal model, sensory model, recurrent neural network, balance control, standing balance, bicycle balance, muscle spindles, fusimotor control, exafferent acceleration feedback, closed-loop feedback control, optimal feedback control, linear quadratic Gaussian, underactuated.*

## Introduction

Goal-directed movements almost always require sensory feedback. For example, standing upright depends on control actions in the form of ankle torques that overcome the toppling torque due to gravity and prevent the body from falling. These control actions are computed by the central nervous system (CNS) and depend on sensory feedback about the body's center of gravity (CoG) relative to its area of support (AoS). The situation is similar in other forms of balance control, such as on the bicycle: the control actions now involve steering (turning the handlebars), and the sensory feedback pertains to the combined CoG of rider and bicycle relative to the line of support (LoS) that is formed by the two contact points between the tires and the road surface.

The difficulty of the CNS's control task depends on the sensory feedback. This can be demonstrated rigorously for a musculo-skeletal system (a human body plus attached objects like a bicycle, a cane, a pencil) that can be modeled as a linear mechanical system. Such a mechanical system is linear if the limb movements are described by differential equations that are linear in the joints' angular positions and velocities, the system's state variables. For balance control, the mechanical system is linear near the so-called fixed point, and for a standing body and a rider-bicycle combination, this fixed point is the upright position. In balance control, the fixed point is above the AoS/LoS, and therefore most of the movements remain close to it, which implies that a linear approximation captures the movements that actually occur. The optimal control action for a linear mechanical system, is a simple linear combination of the state variables [1]. Therefore, the control task for the CNS is simplified if the sensory feedback is an accurate estimate of the state variables: the optimal control action is a simple linear combination of this sensory feedback.

The nature of the sensory feedback is determined by the sensory organs, and this may pose a challenge for the CNS's control task, as is discussed in the next paragraph. For balance control, the contributions of somatosensory

(including proprioceptive), vestibular, visual and auditory feedback have all been investigated [2]. Here, I will focus on proprioceptive feedback from the muscle spindles [3]. There is good empirical evidence that, at least on a firm and immobile support surface, this proprioceptive feedback is sufficient for standing balance control [4-6].

Whether the muscle spindles provide feedback about angular position and velocity (i.e., full state feedback) is a topic of much debate in sensory neurophysiology [7-9]. I will put this debate in a different perspective by only considering a type of sensory feedback about which there is much less controversy (provided by the muscle spindle primary afferents) and will demonstrate that the CNS can compute angular position and velocity from this feedback. For this, the CNS uses an internal sensory model that builds on the fact that, under perfectly coordinated skeletomotor and fusimotor control, the firing rates of muscle spindle primary afferents scale with the exafferent joint acceleration component. This sensory model can be combined with the familiar internal model for the dynamics of the mechanical system [10, 11], and together they specify a dynamical system that estimates the current state. This CNS-internal dynamical system can be implemented as a recurrent neural network (RNN).

The evidence in the present paper comes from formal analysis and computer simulations, and the main point can be made convincingly using the one degree-of-freedom (1-DoF) inverted pendulum model of standing balance control. Focusing on such a simple model has the risk of making general claims about motor control that are only valid for this simple model system. I will therefore make the same point using two 3-DoF models for bicycle balance control. Balancing a bicycle using only proprioceptive feedback is a very challenging control problem because the mechanical system is underactuated [12]: because the rider is not touching the road surface, the bicycle lean angle cannot be directly registered by the muscle spindles nor controlled by a forcing torque over this mechanical joint. I will demonstrate that a bicycle can be balanced using only exafferent acceleration feedback

from the rider's upper body and a steering torque that controls the front frame via the handlebars.

## Results

### A closed-loop feedback control model for standing balance

In Fig. 1A and 1B, a closed-loop feedback control model is shown [13-15]. In its application to standing balance control, the mechanical system (in red) is the body's musculo-skeletal system, which is depicted separately in **Fig. 1C**. This mechanical system is modeled as a compound inverted pendulum (CIP) that rotates about the ankle joint. The pendulum's angular position relative to gravity (lean angle) is denoted by  $\theta$  and the muscular forcing torque at the ankle joint by  $\mathbf{z}$ . The movements of the CIP are fully specified by its equation of motion (EoM), which expresses the acceleration  $\ddot{\theta}$  as a function of position  $\theta$ , velocity  $\dot{\theta}$ , and the forcing torque  $\mathbf{z}$  (see Eq. 3). The EoM is usually written as a function of the mechanical system's state, which is the combined position  $\theta$  and velocity  $\dot{\theta}$ , and is denoted by  $\mathbf{x} = [\theta, \dot{\theta}]^t$ . The distinction between the state

$\mathbf{x}$  and the acceleration  $\ddot{\theta}$  is crucial for balance control because the muscular forcing torque  $\mathbf{z}$  controls  $\ddot{\theta}$  in a direct way, whereas the state variables  $\theta$  and  $\dot{\theta}$  are only controlled indirectly via  $\ddot{\theta}$ . The EoM can be written as a differential equation for the state  $\mathbf{x}$ , which I will denote as  $\dot{\mathbf{x}} = \Phi(\mathbf{x}, \mathbf{z})$ . This differential equation is usually called the EoM in state-space form, and it is described in more detail in *An optimal computational system for a linear approximation of the mechanical system*. (Here and in the following, I will not follow the notational convention of using lower case boldface letters for vectors and normal font for scalars; all results in this paper hold for the vector-valued case, but sometimes the application/example involves only scalars.)



The pendulum's angular position relative to gravity is denoted by  $\theta$  and the torque at the ankle joint by  $\mathbf{z}$ .

The sensory system (in green) linearly maps the vectors  $[\mathbf{x}^t, \ddot{\theta}]^t$  and  $\mathbf{w}$  onto sensory variables, adds noise  $\mathbf{s}$  and feeds the resulting  $\mathbf{y}$  into the computational system. With respect to these sensory variables, I deviate from the existing literature on closed-loop feedback control, where the sensory feedback only pertains to the state variables  $\mathbf{x}$ . The angular acceleration  $\ddot{\theta}$  refers to the total joint acceleration, and the torque variable  $\mathbf{w}$  is used to correct this total acceleration for its re-afferent component. Importantly, the torque variable  $\mathbf{w}$  is direct input from the computational (in blue) into the sensory system (in green). In the muscle spindles, this direct input is implemented by spinal gamma and beta motor neurons (fusimotor neurons) and is denoted as fusimotor control [3, 7, 8]. The motor output system (in black) adds noise to the computational system's output  $\mathbf{u}$ , separately for each of the two pathways: (1) adding motor noise  $\mathbf{m}$  (skeletomotor noise plus external perturbations; see further) produces the noisy torque input  $\mathbf{z}$  into the mechanical system, and (2) adding fusimotor noise  $\mathbf{f}$  produces the noisy torque input  $\mathbf{w}$  into the sensory system.

The sensory, motor, and computational system are models of, respectively, the sensory nervous system, the motor division of the somatic nervous system, and the central nervous system. In this paper, the main interest is in the sensory and the computational system, and I will address the question whether the computational system can control the mechanical system for a plausible sensory feedback and realistic values of the mechanical system's parameters.

From a neurobiological perspective, the computational system is a neural network with an input layer, an intermediate layer with recurrent connections, and an output layer (see Fig. 1A). These recurrent connections agree with the fact that, within the CNS, feedback connections are ubiquitous. As is common in neuroscience, I assume that the CNS learns optimal weights

for the neural network's connections [13-15]. Calculating these optimal weights is a computational challenge which usually is considered a part of machine learning. Here, I take a different approach: I first establish a correspondence between the neural network and the OFC perspective (see Fig. 1B), and then use standard OFC results to express the optimal weights in closed form. From the OFC perspective, the computational system calculates (1) an optimal internal state estimate  $\hat{\mathbf{x}}$  by integrating a linear differential equation that takes the sensory feedback  $\mathbf{y}$  as input, and (2) an optimal control action  $\mathbf{u}$  by multiplying the state estimate  $\hat{\mathbf{x}}$  by the gain  $-K$ .

The computational system is based on (1) a linear forward model  $\dot{\mathbf{x}} = A\mathbf{x} + B\mathbf{z}$  that approximates the nonlinear mechanical system  $\dot{\mathbf{x}} = \Phi(\mathbf{x}, \mathbf{z})$ , and (2) a linear sensory model  $\mathbf{y} = C\mathbf{x} + \mathbf{s}$  of the input to the computational system. I assume the matrices  $A$ ,  $B$  and  $C$  to be given and ask for which values of  $K$  and  $L$  some optimality criterion is achieved. In the time domain, optimality is usually expressed in terms of a loss function, and in the Laplace domain, it is expressed in terms of the poles of a transfer function.

For the claims of the present paper, the exact mathematical specification of the optimality criterion is not required, but for the simulations it is. For these simulations, I will use linear-quadratic-Gaussian (LQG) control [1], which is based on the minimization of the following time domain optimality criterion:

$$J = \lim_{T \rightarrow \infty} \frac{1}{T} \mathcal{E} \left( \int_0^T \{[\mathbf{x}(t) - \mathbf{c}]^t Q [\mathbf{x}(t) - \mathbf{c}] + \mathbf{u}(t)^t R \mathbf{u}(t)\} dt \right) \quad \text{Eq. 1}$$

in which  $\mathcal{E}(\cdot)$  denotes expected value, and  $Q$  and  $R$  are positive definite weight matrices of the appropriate dimensions. This criterion is a quantification of the person's objective to stay balanced with as little effort as possible. The first quadratic form ( $[\mathbf{x}(t) - \mathbf{c}]^t Q [\mathbf{x}(t) - \mathbf{c}]$ ) quantifies the difference between the time-varying state variable  $\mathbf{x}(t)$  and its target state  $\mathbf{c} = [a^+, 0]^t$  (in which  $a^+$  is a small positive number that reflects people's preference for a leaned forward posture), and the second one ( $\mathbf{u}(t)^t R \mathbf{u}(t)$ ) quantifies the energetic cost.

The minimization of  $J$  has a known solution under the following conditions:

(1) the mechanical system is linear and identical to the computational system's forward model (i.e.,  $\dot{\mathbf{x}} = \Phi(\mathbf{x}, \mathbf{z}) = A\mathbf{x} + B\mathbf{z}$ ), (2) the sensory system's output matrix  $C$  is identical to the corresponding matrix of the computational system's sensory model, and (3) the sensor and the motor noise are Gaussian. Optimal control under the LQG is achieved when  $-K$  is the linear quadratic regulator (LQR), which depends on  $A$  and  $B$  (plus the weights  $Q$  and  $R$ ), and  $L$  is the Kalman gain, which depends on  $A$  and  $C$  (plus two noise covariance matrices, which serve as weights) [1].

Applying the LQG results, one can see that the optimal input weights for the neural network in Fig. 1A are the Kalman gain  $L$ , the optimal output weights are the LQR gain  $-K$ , and the optimal recurrent weights are  $A - BK - LC$ . Of course, the CNS can only learn these optimal weights from experience. Because this process develops over time, the weights are never optimal but converge to optimality. To prevent a possible misunderstanding, the equivalence between the neural network in Fig. 1A and the algebraic formalism in Fig. 1B is only used to demonstrate its neural plausibility; no neural network implementation will be built.

It is important to note that the LQG is for continuous signals only, whereas the signals in the peripheral, central and somatic nervous system are sets of spike signals. However, it is possible to formulate a spiking neural network (SNN) with the same functional properties as a LQG controller [16]. This functional equivalence can be demonstrated using a SNN [17, 18] that produces the type of spiking activity that is observed in biological neural networks: irregular, sparse, and robust.

### Incomplete feedback

For a linear mechanical system with observable states  $\mathbf{x}$ , the optimal control action is the linear combination  $-K\mathbf{x}$  [1]. Optimal control actions can also be computed from the sensory feedback when the sensory system's output matrix  $C$  is invertible, namely as  $-KC^{-1}\mathbf{y}$ . Sensory feedback obtained via an

invertible output matrix  $C$  will be called full state feedback, because the mechanical system's states can be obtained from the sensory feedback as  $C^{-1}\mathbf{y}$ . For full state feedback, there is no need to pass it through a recurrently connected intermediate layer such as in Fig. 1A. (It must be noted that "full state feedback" is also used in a different meaning, namely as a method for pole placement in classical control theory.)

If the sensory feedback is not full state, it will be called incomplete. Incomplete feedback can be of different types, such as a non-invertible mapping of the mechanical system's state  $\mathbf{x}$ , or a mapping of non-state variables such as acceleration  $\ddot{\theta}$  and torque  $\boldsymbol{w}$  (see Fig. 1A and 1B). In this paper, I will only focus on the latter type. However, it holds for all types of incomplete feedback that it must be passed through a recurrently connected intermediate layer if it is to be converted into an optimal control action.

Incomplete feedback is not the only use case for a recurrently connected intermediate layer: it will also reduce the effects of motor and/or sensory noise that is added to the input and/or output of the mechanical system. If the sensory feedback is noisy, more accurate state estimates are obtained by combining the noisy sensory feedback with model-based predictions using Bayes' rule [19]. Crucially, this combination can be performed by the RNN in Fig. 1A, and the optimal combination of the noisy sensory feedback with the model-based predictions is realized by the Kalman gain  $L$ . However, for incomplete feedback, the RNN does not simply improve the accuracy of the state estimates: it allows to combine the sensory feedback with the model-based predictions.

## **Muscle spindle proprioceptive feedback**

### *Proprioceptive feedback for balance control*

Balance control relies on contributions from multiple sensory modalities: somatosensory (including proprioception), visual, vestibular and auditory [2, 20-22]. In this paper, I focus on proprioceptive feedback and muscle spindles

are claimed to be the most important sensory organ for this modality [3]. I will formulate a model for balance control that uses only muscle spindle proprioceptive feedback. This is a plausible hypothesis, at least when the support surface is firm and immobile; on such a surface, humans can maintain standing balance after removing vestibular, touch, and visual feedback [4-6].

### *What feedback is generated by muscle spindles?*

It is a common assumption in the field of standing balance control that muscle spindles provide feedback about angular position and velocity [2, 22, 23]. However, the nature of muscle spindle afferent feedback is a topic of debate in sensory neurophysiology: two specialized review papers argue against the claim that the spindles provide feedback about angular position and velocity [7, 8], and one argues in favor of it [9]. Central to this debate is the existence of two types of spindle afferents: the primary (type Ia) and the secondary (type II) afferents. There is consensus that primary spindle afferents do not reliably encode position and velocity, and the strongest empirical evidence comes from studies in which the spindle-containing muscle has to act against a load [24-29]: primary afferent firing rates scale with load, not with joint angular position. This is highly relevant for balance control, which involves acting against a gravitational load.

Given the consensus on the primary afferents, the debate focuses on whether secondary afferents reliably encode position and velocity. However, in this paper, I will only consider primary afferents, and this is for three reasons. First, primary afferents are much more responsive to the dynamics of the stretch, as is reflected in their high sensitivity to acceleration [7, 30]. A high sensitivity to acceleration is especially beneficial if the position variable has a small amplitude, which is the case in balance control; the body sway/lean angular position amplitude is smaller by an order of magnitude than the joint angular position amplitudes that were used to demonstrate the secondary afferents' position sensitivity [9]. Second, it is highly unlikely that the CNS uses joint-specific angular positions or velocities for bicycle balance control,

because humans achieve this without muscle spindles that can inform the CNS about the joint between the rear wheel and the road surface (which is non-biological). This is the most important mechanical joint for bicycle balance control. Third, I want to use this paper to make a case for the CNS as the organ where position and velocity information is generated. This contrasts with many sensory neurophysiology studies whose aim is to demonstrate that control-relevant sensory variables are already present in the output of the sensory organs. In other words, I want to demonstrate that the body lean angle position and velocity can be a computed instead of registered.

### *Muscle spindle anatomy and physiology*

A muscle spindle contains the endings of the sensory neurons, and these terminate at so-called intrafusal fibers, which have a sensory function only; the contractile force is produced by the muscle's extrafusal fibers. The sensory neurons' endings respond to the stretch in the intrafusal fibers and if they lie slack (zero tension), the sensory neuron provides no information about the muscle's extrafusal fibers. The primary and the secondary spindle afferents terminate at different parts of the intrafusal fibers: the primary afferents terminate at the central region of the intrafusal fibers, and the secondary afferents terminate adjacent to this central region.

The response properties of muscle spindles are investigated using direct recordings of their output, afferent spikes in sensory neurons. In anesthetized animals, such recordings are obtained from the dorsal horn of the spinal cord [31], and in awake humans from sensory axons using microneurography [7, 32]. One of the main results of human microneurography pertain to the differences between passive and active joint movements: in a passive joint (i.e., a joint that is moved by the experimenter), spindle afferents provide length and velocity information, but this is no longer the case if this joint is actively moved [7].

A crucial difference between the active and the passive muscle is that, in the former, the muscle spindle intrafusal fibers are activated by spinal fusimotor neurons as a part of fusimotor control. Without fusimotor control, muscle spindle output would only depend on the length of the extrafusal fibers that determine the joint's position. The simplest form of fusimotor control is alpha-gamma coactivation, which effectively deals with the problem that the stretch-sensitive sensory endings have a limited operating range: when the extrafusal fibers contract, the tension in the intrafusal fibers can become too low (they fall slack) for the sensory endings to fire, regardless of the length/velocity/acceleration of the extrafusal fibers. Fusimotor neurons control the length of the intrafusal fibers, and thereby the sensitivity/gain of the sensory neurons. In alpha-gamma coactivation, the gamma motor neurons fire in sync with the spinal alpha motor (skeletal motor) neurons, whose firing makes the extrafusal fibers contract. This coordination keeps the intrafusal fibers at a length that keeps the sensory neurons in their operating range.

More complicated forms of fusimotor control have been described and they all involve CNS-level computations that allow for temporal coordination between fusimotor and skeletal motor neurons [8, 33, 34]. Here, I focus on the role of this temporal coordination in distinguishing between reafferent and exafferent feedback. The better the temporal coordination, the more the sensitivity of the sensory neurons shifts to non-muscular forces such as gravity, elasticity (which both depend on angular position) and damping (which depends on angular velocity). If the coordination is perfect, then the net forces acting on the intrafusal fibers do not reflect the extrafusal fiber contractions, and the muscle spindle output thus only reflects non-muscular forces. In other words, the muscle spindle feedback is purely exafferent. Because fusimotor axons have a lower conduction velocity as compared to skeletal motor axons, temporal coordination between fusimotor and skeletal motor neural activity may require a dual delay compensation.

In the next section, I will describe the evidence for this hypothesis and will show how the computational system can extract position- and velocity-related information from these exafferent accelerations.

### **A mechanical model for standing balance constrains the relation between intrafusal fiber acceleration and the state variables**

#### *A mechanical model specifies acceleration components*

I now describe a mechanical model for standing balance (the CIP) that can be used to specify the acceleration component to which the spindle primary afferents respond. The CIP EoM is the following second-order differential equation:

$$M\ddot{\theta} + c_{damp}\dot{\theta} - \frac{1}{2}mgl \sin(\theta) + k_{stiff} \theta = z , \quad \text{Eq. 2}$$

in which  $m$  is the mass of the compound pendulum,  $l$  is its length, and  $g$  is the gravitational constant. The constant  $M$  denotes the mass moment of inertia  $M = \frac{1}{3}ml^2$ ; it is denoted by a capital letter to distinguish it from the mass  $m$  and for consistency with the matrix form of the mass moment of inertia that will be introduced in a later section. The ankle joint has both stiffness and damping, and these are characterized by the coefficients  $k_{stiff}$  and  $c_{damp}$ . The variable  $z$  is the forcing torque applied at the ankle. This forcing torque is produced by the muscles' extrafusal fibers and is the sum of a control signal plus motor noise. A critical aspect of Eq 2 is the relation between  $k_{stiff}$  and the critical stiffness  $\frac{1}{2}mgl$ : if  $k_{stiff} < \frac{1}{2}mgl$ , the CIP is unstable in the upright position ( $\theta$  accelerates away from 0), and if  $k_{stiff} > \frac{1}{2}mgl$ , it is stable. Several studies have demonstrated that the ankle joint stiffness  $k_{stiff}$  is less than the critical stiffness  $\frac{1}{2}mgl$ , and that this is due to the compliance of the Achilles tendon [35-38].

I rewrite Eq. 2 by (1) bringing the state variables to the right side of the equation, and (2) dividing both sides by the mass moment of inertia  $M$ :

$$\ddot{\theta} = M^{-1} \left[ -c_{damp} \dot{\theta} + \frac{1}{2} mgl \sin(\theta) - k_{stiff} \theta + z \right] \quad \text{Eq. 3}$$

All terms in Eq. 3 are acceleration components: the terms containing  $\dot{\theta}$ ,  $\sin(\theta)$ ,  $\theta$ , and  $z$  are the acceleration components that are due to, respectively, damping, gravity, elasticity, and the forcing torque, and  $\ddot{\theta}$  is the total acceleration. Eq. 3 imposes a constraint on the relation between the variables  $\theta$ ,  $\dot{\theta}$ ,  $\ddot{\theta}$  and  $z$ , and the computational system can make use of this constraint to extract information about the state variables  $x = [\theta, \dot{\theta}]^t$  from acceleration feedback.

The differential equation in Eq. 3 pertains to a joint that is controlled by multiple muscles, and these are usually grouped functionally as agonists and antagonists. I define the agonists and antagonists as the muscles that produce positive, respectively, negative torque. This implies that the forcing torque  $z$  in Eq. 3 is the net torque that results from the combined action of agonists and antagonists.

#### *One-to-one correspondence between angular and translational accelerations*

Eq. 3 can be used to specify the acceleration components that are registered by the spindles in the muscles that cross the joint at which the forcing torque  $z$  is produced (both agonists and antagonists). Note first that Eq. 3 involves an angular acceleration  $\ddot{\theta}$  whereas the spindle primary afferents respond to translational accelerations in the agonist and antagonist muscles. However, for a given joint, there is a one-to-one correspondence between the joint's angular acceleration  $\ddot{\theta}$  and the translational accelerations in the associated muscle-tendon units. The relevant equations depend on the moment arms (i.e., the location of the tendons' attachment to the joint's bones), but there is no need to specify this in more detail.

I assume that the translational acceleration in a muscle-tendon unit is dominated by the acceleration in the muscle's extrafusal fibers. This implies that the tendon may not be so compliant that the muscle's acceleration is absorbed in the tendon. We know that the Achilles tendon is too compliant to

keep the body mass over the body's AoS [35-38], but it may not be so compliant that the muscle's acceleration does not dominate the acceleration of the muscle-tendon unit. Under this assumption, there is a one-to-one correspondence between the joint's angular acceleration and the translational accelerations in the associated extrafusal fibers. In the Discussion, I will discuss the consequences of a muscle-tendon unit with a larger tendon compliance.

For four scenarios, I will now describe how Eq. 3 can be used to specify the acceleration components that are registered by the spindle primary afferents: (1) a passively accelerating joint, (2) an actively accelerating joint, (3) a joint under external perturbations, and (4) an active stationary joint (isometric contraction).

#### *Scenario 1: A passively accelerating joint*

Because the muscles are passive in this scenario, there is no fusimotor control. Therefore, the linear accelerations of the extra- and the intrafusal fibers are identical, and the one-to-one correspondence also holds between  $\ddot{\theta}$  and the translational acceleration of the intrafusal fibers. Because the intrafusal fiber accelerations determine the spindle firing rates, there also is a one-to-one correspondence between  $\ddot{\theta}$  and the spindle firing rates in the muscles that are stretched in this acceleration.

For a 1 degree of freedom joint, the neural signal that reflects the angular acceleration  $\ddot{\theta}$  is the difference between the firing rates that originate from two populations of sensory neurons, one providing information about the agonist and the other about the antagonist muscle. The firing rates in these populations reflect the positive acceleration in their corresponding muscle, and their difference thus encodes the angular acceleration  $\ddot{\theta}$ .

*Scenario 2: An actively accelerating joint*

For this scenario, I assume perfectly coordinated fusimotor and skeletomotor control. I rewrite Eq. 3 by bringing the forcing torque to the left side:

$$\ddot{\theta} - M^{-1}z = M^{-1} \left[ -c_{damp}\dot{\theta} + \frac{1}{2}mgl \sin(\theta) - k_{stiff} \theta \right] \quad \text{Eq. 4}$$

In this scenario, the neural signal that informs the CNS about the CIP state is proportional to  $\ddot{\theta} - M^{-1}z$ . The term  $M^{-1}z$  is the contribution of the forcing torque  $z$  to the total joint angular acceleration  $\ddot{\theta}$ , which is related one-to-one to linear accelerations in the agonist and the antagonist extrafusal fibers.

Without fusimotor activity, these accelerations would also be present in the intrafusal fibers and would thus cause reafferent feedback. I now assume that the fusimotor neurons generate an acceleration in the intrafusal fibers that cancels this reafferent feedback. Although this intrafusal fiber acceleration is linear, I will represent it by the angular acceleration  $-M^{-1}z$  from which the linear accelerations in the agonist and antagonist muscle spindle can be calculated. By taking the difference  $\ddot{\theta} - M^{-1}z$ , the reafferent feedback is removed from the total acceleration  $\ddot{\theta}$ , and this results in pure exafferent feedback. This agrees with the fact that the right side of Eq. 3 expresses the same quantity but now as a function of angular position and velocity, which determine the non-muscular forces gravity, elasticity, and damping. These non-muscular forces are responsible for the exafferent feedback.

For biological plausibility, I now relax the assumption that the fusimotor neurons generate an acceleration  $-M^{-1}z$  in the intrafusal fibers that exactly cancels the reafferent feedback. To allow for the fusimotor and the skeletomotor system to generate a different noise, I assume that the fusimotor neurons generate an intrafusal fiber acceleration  $-M^{-1}w = -M^{-1}(u + f)$ , in which  $f$  is the fusimotor noise (see Fig. 1A and 1B). The quantity  $M^{-1}w$  is the predicted reafferent acceleration. In the presence of fusimotor noise, the intrafusal fiber acceleration is  $\ddot{\theta} - M^{-1}w$ . Starting from Eq. 4, after some rewriting, this noisy intrafusal fiber acceleration (IFA) can be written as a function of  $\theta$ ,  $\dot{\theta}$ ,  $m$ , and  $f$ :

$$IFA(\theta, \dot{\theta}, m, f) = \ddot{\theta} - M^{-1}w$$

$$= M^{-1} \left[ -c_{damp} \dot{\theta} + \frac{1}{2} mgl \sin(\theta) - k_{stiff} \theta + m - f \right]$$

The noise in the IFA is the sum of a term that depends on motor noise ( $M^{-1}m$ ) and one that depends on fusimotor noise ( $-M^{-1}f$ ). With identical motor and fusimotor noise (i.e.,  $f = m$ ), the IFA is noise-free, and this drastically improves the performance of the model in the simulations (results not shown). In this paper, I only consider the case  $f \neq m$ , which corresponds to imperfect alpha-gamma coactivation. Besides the motor and the fusimotor noise terms, the sensory feedback  $y$  also contains a term that reflects the noise in the transduction of the IFA into neuronal firing rates (see the  $s$  in Fig. 1B). With respect to the performance of the model, this transduction noise  $s$  cannot be distinguished from the fusimotor noise term  $M^{-1}f$ .

The reasoning in the previous paragraph is fully in line with [8, 33, 34] who argued that muscle spindles can be tuned by the CNS via its innervation of the spinal fusimotor neurons. Importantly, the subtraction of the predicted reafferent feedback goes beyond simple alpha-gamma coactivation which operates at the level of a single muscle. Instead, it is proposed that the CNS combines the planned muscle activations affecting a given joint (both agonists and antagonists) and cancels the resulting reafferent feedback via fusimotor neurons.

$IFA(\theta, \dot{\theta}, m, f)$  encodes three variables: angular position  $\theta$ , velocity  $\dot{\theta}$ , and acceleration (the latter via the noise torques  $m$  and  $f$ ). Angular position  $\theta$  is encoded via the gravitational and the elastic force  $\left[ \frac{1}{2} mgl \sin(\theta) - k_{stiff} \theta \right]$ , which are proportional to  $\theta$  after linearizing  $\sin(\theta)$ . And angular velocity  $\dot{\theta}$  is encoded via the damping/viscous force  $-c_{damp} \dot{\theta}$ , which is proportional to  $\dot{\theta}$ . The spindle primary afferent firing rates are proportional to this IFA, and this resolves the apparent contradiction between (1) the muscle spindle being a stretch receptor, responding to force, and (2) the spindle providing information about position and velocity.

*Scenario 3: A joint under external perturbations*

External perturbations have been used to investigate the kinematic signal that drives the corrective response [39-41]. The model predicts that corrective responses to external perturbations are driven by acceleration, and this is also what has been found for external perturbations of standing balance [39-41]. Crucially, this acceleration-driven component in the corrective responses depends on proprioceptive feedback, because it is only present in animals with intact proprioceptive afferents [39].

The fact that corrective responses to an external perturbation are driven by acceleration does not yet demonstrate that these responses are also successful in restoring balance. Here lies a contribution of the proposed model because  $IFA(\theta, \dot{\theta}, m, f)$  not only depends on the external perturbation via the motor noise  $m$  but also via the state variables  $\theta$  and  $\dot{\theta}$ . The mechanical system acts as a low-pass filter of the perturbing torque, and thus its effect on the state variables  $\theta$  and  $\dot{\theta}$  remains present for a longer time than the motor noise itself. Because  $IFA(\theta, \dot{\theta}, m, f)$  also depends on  $\theta$  and  $\dot{\theta}$ , the sensory feedback continues to provide balance-relevant information when the perturbing torque is no longer present.

*Scenario 4: An active stationary joint*

In this scenario, the joint is not moving but one muscle is actively contracting against an external load (isometric contraction). This scenario is typical for standing balance because people prefer a leaned forward posture. In this position, the calf muscles produce a torque that acts against the gravitational torque that results from this posture. In this scenario,  $\ddot{\theta} = 0$  and  $\dot{\theta} = 0$ , from which follows that

$$\begin{aligned} IFA(\theta, \dot{\theta}, m, f) &= M^{-1}w \\ &= M^{-1} \left[ \frac{1}{2}mgl \sin(\theta) - k_{stiff} \theta + m - f \right] . \end{aligned}$$

The term  $M^{-1} \left[ \frac{1}{2}mgl \sin(\theta) - k_{stiff} \theta \right]$  is the IFA that would be observed if there was no muscular torque acting against the net gravitational torque

(gravitational torque corrected for stiffness). In the presence of a counteracting muscular torque (the current scenario), the IFA reflects the tension in the intrafusal fibers.

The model predicts that keeping the joint stationary against an external load produces spindle primary afferent firing rates that are proportional to this load. This prediction is in exact agreement with human microneurography experiments involving stationary joints acting against an external load [24, 25]. These spindle primary afferent firing rates under load are even observed in a slowly contracting muscle [26, 27, 29].

In sum, spindle primary afferent firing rates scale with the acceleration that is produced by the non-muscular forces (accelerating joint scenario), or that would be produced if there was no muscular force working against an external load (stationary joint scenario). The role of fusimotor control is creating the appropriate tension in the intrafusal fibers such that pure exafferent feedback is generated. This exafferent feedback reflects either actual (accelerating joint) or possible (stationary joint) acceleration, but in both scenarios, it scales with the non-muscular forces.

*How does the computational system extract state information from the IFA?*

The IFA depends on both joint angular position, velocity, and acceleration. Because these components are not separated within the sensory organ (i.e., there are no separate channels for position, velocity, and acceleration), the resulting feedback is incomplete. I now describe how the computational system can extract state information from this mixture of signals.

I assume that the computational system uses a linear approximation of the nonlinear CIP, and I therefore linearize the right side of Eq. 4 (using  $\sin(\theta) \approx \theta$  for  $\theta \approx 0$ ). In the approximation, I also ignore the consequences of noise and therefore, on the left side of Eq. 4, I replace  $z$  by  $w$ :

$$\ddot{\theta} - M^{-1}w \approx M^{-1} \left[ -c_{damp}\dot{\theta} + \left( \frac{1}{2}mgl - k_{stiff} \right) \theta \right]$$

In matrix notation:

$$\begin{bmatrix} 1 & -M^{-1} \end{bmatrix} \begin{bmatrix} \ddot{\theta} \\ w \end{bmatrix} \approx \begin{bmatrix} M^{-1} \left( \frac{1}{2} mgl - k_{stiff} \right) & -M^{-1} c_{damp} \end{bmatrix} \begin{bmatrix} \theta \\ \dot{\theta} \end{bmatrix} \quad \text{Eq. 5}$$

The coefficient matrix on the left side of Eq. 5 is the green matrix  $C$  in the sensory system of Fig. 1A and 1B, and the coefficient matrix on the right side is the blue matrix  $C$  in Fig. 1B. Denoting these two matrices by, respectively,  $C_{Sens}$  and  $C_{Comp}$ , one obtains

$$C_{Sens} \begin{bmatrix} \ddot{\theta} \\ w \end{bmatrix} \approx C_{Comp} \begin{bmatrix} \theta \\ \dot{\theta} \end{bmatrix} = C_{Comp} \mathbf{x}$$

Thus, there exists a linear combination of the sensory feedback variables  $\ddot{\theta}$  and  $w$  that equals a linear combination of the state variables  $\mathbf{x}$ . The matrix product  $C_{Comp} \mathbf{x}$  is a sensory internal model [42].

Because  $C_{Comp}$  is not invertible, the important question is whether the computational system can estimate every state from a time history of this incomplete sensory feedback. In control theory, this property is known as observability, and for a linear system it can be assessed from the row space of the so-called observability matrix [43]. Unfortunately, this matrix condition does not tell us whether the mechanical system of interest (the standing body) can be controlled with realistic state and control variables (body angular position, angular velocity, and ankle torques) and realistic noise levels. In this paper, I will use simulation to evaluate whether sensory feedback governed by the matrix pair  $[C_{Sens}, C_{Comp}]$  is sufficient for standing balance control.

### **An optimal computational system for a linear approximation of the mechanical system**

I now describe how to simulate the model in Fig. 1B, and to use these simulations to test whether sensory feedback governed by the matrix pair  $[C_{Sens}, C_{Comp}]$  is sufficient for standing balance control. The rationale for this test is the following: if an optimal computational system with sensory model  $C_{Comp} \mathbf{x}$  cannot control the CIP with a realistic body sway and ankle torque, then we can rule out the hypothesis that the matrix pair  $[C_{Sens}, C_{Comp}]$  is

sufficient for standing balance control. Note that this rationale does not hold if the computational system were suboptimal.

The starting-point are the nonlinear CIP EoM in state-space form, which follow from Eq. 3:

$$\begin{aligned}\dot{\mathbf{x}} = \begin{bmatrix} \dot{\theta} \\ \ddot{\theta} \end{bmatrix} &= \begin{bmatrix} \dot{\theta} \\ M^{-1} \left( -c_{damp} \dot{\theta} + \frac{1}{2} mgl \sin(\theta) - k_{stiff} \theta + z \right) \end{bmatrix} \\ &= \Omega(\mathbf{x}, z)\end{aligned}$$

A linear approximation of  $\Omega(\mathbf{x}, z)$  is obtained by taking the first order Taylor expansion around 0 (for  $\theta$ ,  $\dot{\theta}$  and  $z$ ):

$$\begin{aligned}\dot{\mathbf{x}} &\approx \begin{bmatrix} 0 & 1 \\ M^{-1} \left( \frac{1}{2} mgl - k_{stiff} \right) & -M^{-1} c_{damp} \end{bmatrix} \mathbf{x} + \begin{bmatrix} 0 \\ M^{-1} \end{bmatrix} z \\ &\approx A\mathbf{x} + Bz\end{aligned}\quad \text{Eq. 6}$$

Note that  $Bz = B(u + m) = Bu + Bm$ , which implies that the system noise ( $Bm$ ) is a linear function of the motor noise. This follows from the assumption that the mechanical system is deterministic for a given input  $z$  because, in that case, the noise in the system's output only depends on the noise in its input.

I now consider optimal control in the sense of Eq. 1 for the following linear dynamical system:

$$\begin{aligned}\dot{\mathbf{x}} &= A\mathbf{x} + Bu + Bm \\ y &= C_{Comp}\mathbf{x} + M^{-1}m - M^{-1}f + s\end{aligned}$$

with Gaussian motor ( $m$ ) and sensor ( $s$ ) noise. This optimal control problem is a LQG and its solution is given by a linear differential equation that governs the state estimates  $\hat{\mathbf{x}}$ :

$$\dot{\hat{\mathbf{x}}} = (A - BK)\hat{\mathbf{x}} + L(y - C_{Comp}\hat{\mathbf{x}}) \quad \text{Eq. 7}$$

in which  $-K$  is the LQR gain and  $L$  is the Kalman gain, and the control signal  $u$  equals  $-K\hat{\mathbf{x}}$  [1]. This is the standard solution of the LQG with a few adaptations to the usual way of calculating the Kalman gain: (1) the system noise covariance scaling matrix equals  $B\text{var}(m)B^t$  and thus depends on  $B$ , (2) the sensor noise covariance scaling matrix contains a term that depends

on the fusimotor noise (i.e.,  $M^{-1}\text{var}(f)M^{-1^t}$ ), and (3) the system and the sensor noise are correlated because the motor noise appears in both the state and the output equation, and the motor the fusimotor noise can be correlated.

### **Standing balance can be controlled using exafferent ankle joint acceleration feedback**

I now report on a simulation study that evaluates whether OFC with exafferent acceleration feedback can control standing balance with realistic model parameters and realistic kinematic simulation output. In this section, I give a general description of the simulation study; details are given in the Methods. First, the mechanical system (the CIP) is specified by realistic and/or empirical values for its parameters (body length and mass, stiffness, damping). Second, the simulations require noise input and I set the amplitudes of the motor and the fusimotor noise such that their combined effect on the sensory feedback roughly matches the effect of the pure sensory noise: I set the motor noise amplitude such that its contribution to the noise in the sensory feedback equals half the contribution of the pure sensory noise, and I then set fusimotor noise amplitude equal to the motor noise amplitude. The shared variance of the motor and the fusimotor noise is 50%. Third, the LQR gain depends on the weights of the optimality criterium in Eq. 1 (the 2-by-2 matrix  $Q$  and the scalar  $R$ ) and these are set such that the precision ( $Q$ -dependent) and the energetic cost ( $R$ -dependent) component have an equal contribution to the optimality criterium.

In the human neuromuscular system, every joint has a torque limit, and I therefore ran simulations in which the output of the computational system was truncated at an empirically determined maximum torque. The maximum ankle torque was set at 195 Nm [44]; if the computational system requested a higher torque value  $u$ , it was replaced by this maximum.

There are two requirements for a plausible balance control model: (1) the angular position root-mean-square deviation (RMSD) must converge to zero

with decreasing noise amplitude, and (2) the whole RMSD range that is observed empirically must also be produced by the model. There are two empirically determined RMSD maxima, each one corresponding to some noise level: (1) the maximum noise/RMSD for which the computational system can keep the mechanical system's CoG within its AoS (see Methods), and (2) the maximum noise/RMSD that humans will tolerate. This second maximum was obtained from a study in which participants had to rely on proprioceptive feedback only (vestibular loss patients with their eyes closed); these participants did not tolerate an angular position RMSD above 1.5 degrees [23, Fig. 4]. For the model to be plausible, the RMSD for which the computational system can keep the mechanical system's CoG within its AoS must be less than 1.5 degrees.

Sample results of the simulations are shown in Fig. 2. Panel A shows that (1) the angular position RMSD converges to zero with decreasing noise amplitude, and (2) the CoG moves outside the AoS for a noise level with an angular position RMSD that exceeds the one that can still be tolerated. This result depends on settings (relative noise amplitudes, weights of the LQR optimality criterium) that are not fully motivated by empirical results, but it is robust to variations within an order of magnitude, especially for the LQR optimality criterium (results not shown).

Panel B shows the angular position power spectral density (psd) for the noise scale that is marked by a "V" in Panel A. Its shape is remarkably similar to the average psd obtained in a large group of healthy participants [see Fig. 1 in 45]. Panel C shows an example angular position time series for the same noise scale as Panel A. Note the asymmetry around the target angular position, which is a consequence of the gravitational torque pulling the body forward when it is at its target angular position.

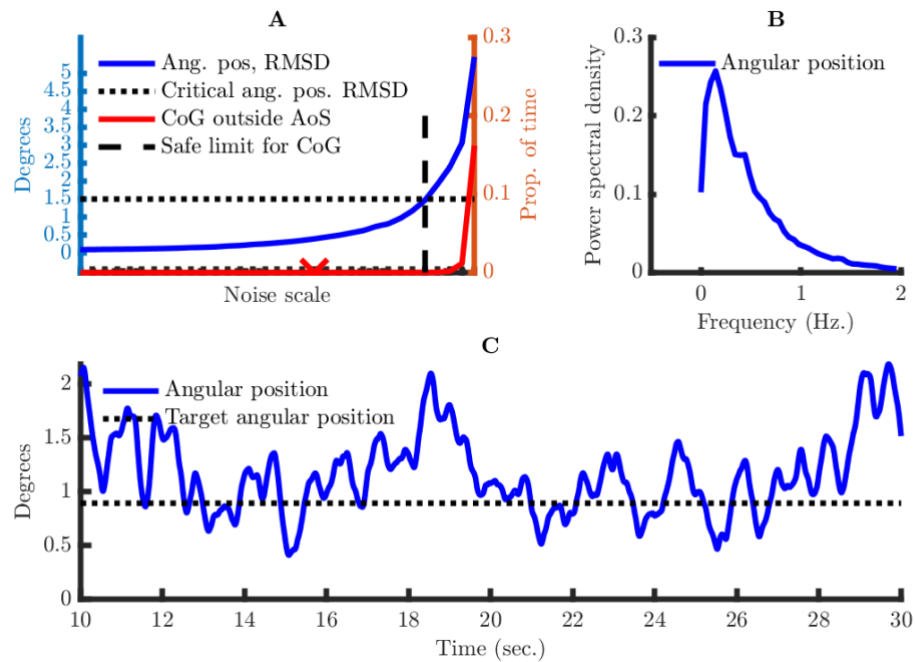


**Fig. 2: Simulation results for standing balance control using exafferent acceleration sensory feedback.** (A) Two indices of lack of control as a function of noise: angular position RMSD and the proportion of the time that the angular position exceeds its critical values. The horizontal dotted line indicates the maximum RMSD based on [23], and the vertical dashed line indicates the first noise amplitude for which the computational system cannot keep the mechanical system's CoG within its AoS. (B) Power spectral density of the angular position for the noise scale that is indicated by a red V in panel A. (C) Example angular position time series for the same noise scale as in B.

This simulation study shows that exafferent joint acceleration feedback is sufficient for controlling standing balance in a realistic way: using realistic parameters for the mechanical system, the computational system keeps the CoG angular position in a realistic regime with respect to angular position RMSD and spectral content.

### Bicycle balance control

I will demonstrate that a bicycle can be balanced using exafferent joint acceleration feedback from the rider's upper body.

*Problem definition and bicycle mechanics*

There are two important differences between standing and bicycle balance control: (1) a bicycle's AoS is a line instead of a surface, and (2) balance control of a moving bicycle involves not only the gravitational but also the centrifugal force. A stationary bicycle is balanced when the combined CoG of rider and bicycle is above the line that connects the contact points of the two wheels with the road surface, the so-called line of support (LoS). Because of disturbances, this CoG cannot be exactly above this one-dimensional LoS for some time. Therefore, a bicycle is considered balanced if the CoG fluctuates around the LoS within a limited range, small enough to prevent the bicycle from touching the road surface.

On a moving bicycle, not only gravity, but also the centrifugal force acts on the CoG. Crucially, the centrifugal force is under the rider's control via the turn radius [46]. The balance of a moving bicycle depends on the resultant of all forces that act on the CoG: a bicycle is balanced if the direction of this resultant force fluctuates around the LoS within a fixed range. Besides the forces that act on the CoG, there are also forces that are responsible for the turning of the bicycle's front frame, and some of these forces are independent of the rider's actions [47]. These rider-independent forces are responsible for the bicycle's self-stability and will not be described in detail.

For investigating bicycle balance control, I use the bicycle model in Fig. 3. This model consists of three rigid bodies: front frame, rear frame, and the rider's upper body. The rear frame includes the lower body and will also be denoted as the lower body. The positions of these three bodies are specified by three angular variables: steering ( $\delta$ ), lower body ( $\theta_1$ ), and upper body ( $\theta_2$ ) angular position. The lower and upper body angular positions are relative to gravity.

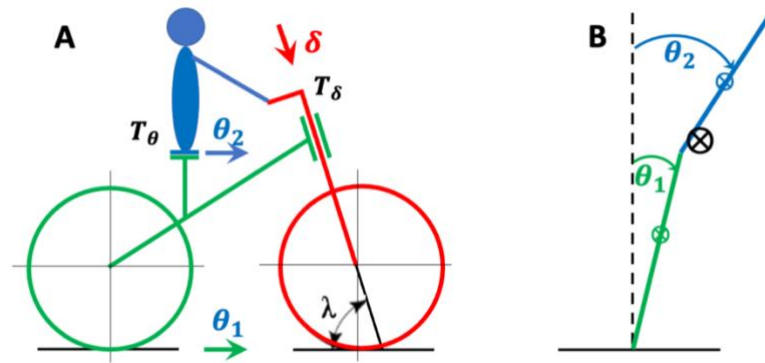


**Fig 3: Kinematic variables of the bicycle model plus the rider-controlled forcing torques.** (A) Side view. In green, the bicycle rear frame, characterized by its angular position  $\theta_1$  over the roll axis (green arrow). In red, the bicycle front frame, characterized by its angular position  $\delta$  over the steering axis (red arrow). In blue, the rider's upper body, characterized by its angular position  $\theta_2$  over the roll axis (blue arrow). In black, (1) the steering torque  $T_\delta$  and the pelvic torque  $T_\theta$ , which are both applied by the rider, and (2) the steering axis angle  $\lambda$  (see text). (B) Rear view. In green, the bicycle rear frame (including the lower body) angular position  $\theta_1$ . In blue, the rider's upper body angular position  $\theta_2$ . The symbol  $\otimes$  denotes the CoG of the upper body (in blue), the lower body (in green), and the combined CoG (in black).

Cycling involves a double balance problem, of which I have only described the first part, which is keeping the combined CoG of rider and bicycle above the LoS. The second balance problem pertains to the rider's upper body only, and it involves keeping the upper body CoG above its AoS, the saddle. I will only consider the balance over the roll axis (parallel to the LoS), which corresponds to upper body movements to the left and the right. I thus ignore the balance over the pitch axis (perpendicular to the LoS and gravity), which corresponds to upper body movements to the front and the back, typically caused by accelerations and braking.

For both balance problems (with respect to the combined and the upper body CoG), the relevant control actions must result in a torque over the roll axis. Within the constraints of our kinematic model, there are two possible control actions: (1) turning the handlebars (using steering torque  $T_\delta$ ), and (2) leaning the upper body (using pelvic torque  $T_\theta$ ). At this point, it is

convenient to make use of Fig. 3B, which is a schematic of a double compound pendulum (DCP). By turning the handlebars, the contact point of the front tire (represented by the green rod) with the road surface moves to the left or the right, and this changes the position of the combined CoG relative to the LoS. In the bicycle reference frame (in which the LoS is one of the axes) this corresponds to a centrifugal torque in the direction opposite to the turn (a tipping out torque). Steering in the direction of the lean produces a tipping out torque that brings the combined CoG over the LoS. This is called steering to the lean/fall.

The second control action is leaning the upper body, which can bring the upper body CoG above the saddle in a direct way. This deals with the second balance problem. However, there is consensus that leaning the upper body cannot deal with the first balance problem (bringing the combined CoG above the LoS), at least not in a direct way. An important argument in favor of this view is that a bicycle with a locked steer cannot be balanced; not a single case has been reported. However, leaning the upper body can deal with the first balance problem in an indirect way: leaning the upper body to one side will make the front and the rear frame lean to the other side (by conservation of angular momentum). Depending on geometrical properties of the bicycle, this rear frame lean may turn the front frame to the same side [47, 48].

*What sensory information informs the CNS about the combined CoG angular position?*

One of the most challenging aspects of bicycle balance control pertains to the sensory feedback that informs the CNS about the combined CoG angular position. To describe this, I now make use a relation between  $C_{Sens}$  and  $C_{Comp}$  that holds for a general multibody mechanical system, and that is derived in the Methods. From this derivation, it is convenient to repeat Eq. 11:

$$\tau = M(\mathbf{q})^{-1} H[\ddot{\theta}] \approx \tau_{Comp}(\mathbf{q}, \dot{\mathbf{q}})[\theta]$$

$$C_{Sens} \begin{bmatrix} \ddot{\boldsymbol{\theta}} \\ \mathbf{z} \end{bmatrix} \approx C_{Comp} \begin{bmatrix} \boldsymbol{\theta} \\ \dot{\boldsymbol{\theta}} \end{bmatrix}$$

The symbols in this equation map onto the ones in Fig. 3 as follows:  $\boldsymbol{\theta} = [\delta, \theta_1, \theta_2]^t$  and  $\mathbf{z} = [T_\delta, T_\theta]^t$ . Note that the joint between the lower body (rear frame) and the road surface is not actuated, and thus there is no torque that corresponds to  $\theta_1$ . Because our bicycle model has less actuators than degrees of freedom, it belongs to the category of underactuated systems [12]. To control a non-actuated joint, an underactuated system must rely on the actuated joints, and this may be a challenging task for the controller.

The matrices  $C_{Sens}$  and  $C_{Comp}$  have order 3x5 and 3x6, respectively. Via the term  $I\ddot{\boldsymbol{\theta}}$ , every row in  $C_{Sens}$  and  $C_{Comp}$  corresponds to one of the three joints of the bicycle model: the steering joint ( $\ddot{\delta}$ ), the joint between the road and the lower body ( $\ddot{\theta}_1$ ), and the pelvic joint ( $\ddot{\theta}_2$ ). With respect to proprioceptive feedback at the pelvic joint, only the difference acceleration  $\ddot{\theta}_2 - \ddot{\theta}_1$  can be registered (see Fig. 3B). This fact requires matrices  $C_{Sens}$  and  $C_{Comp}$  with two rows, of which one corresponds to  $\ddot{\delta}$  and the other to the difference acceleration  $\ddot{\theta}_2 - \ddot{\theta}_1$ . This is obtained by pre-multiplying the original  $C_{Sens}$  and  $C_{Comp}$  by the following matrix:

$$\begin{bmatrix} 1 & 0 & 0 \\ 0 & -1 & 1 \end{bmatrix}$$

Thus, no unique information about the angle between the road and the lower body enters the computational system; the corresponding joint is not only non-actuated, but it also sends no unique information about its state to the computational system.

During normal cycling, the lower body is used for propulsion, but it cannot be ruled out that resting on the pedals allows to register balance-relevant sensory information. Therefore, for the purpose of this paper, I consider a restricted form of cycling in which the rider keeps his legs still, does not use them to carry weight, and relies on a motor for propulsion. This is like balance control on a scooter.

I will test the hypothesis that a bicycle can be balanced using the same type of proprioceptive feedback as for standing balance control. The latter involves exafferent ankle joint accelerations over the same axis as the angular position that the person wants to control. In bicycle balance control, there are two controllable joints, the steering axis and the pelvis, but only the latter is over the same axis as the CoG angular position that the rider wants to control. Thus, to test the hypothesis that a bicycle and a standing body can be balanced using the same type of feedback, I ignore the exafferent acceleration feedback from the steering axis. In the simulations on which I will report, this was implemented by pre-multiplying the original  $C_{Sens}$  and  $C_{Comp}$  by the vector  $[0 \quad -1 \quad 1]$ , which also turns them into vectors. As expected, including the steering axis feedback in the simulations (i.e., using the pre-multiplication matrix with two rows) improved the performance of the controller (results not shown). The reported simulation results are thus for a suboptimal scenario, but with the same type of feedback as for standing balance control.

To the best of my knowledge, there is no empirical evidence for the hypothesis that pelvic joint proprioceptive feedback is sufficient for bicycle balance control. However, there are observations that suggest that a bicycle cannot be balanced if the pelvic joint proprioceptive feedback cannot be processed correctly by the rider's internal models. These observations come from a study in which riders were instructed to take turns with a special bicycle (a bricycle) that, on initiation of a turn, tips the rear frame to the outside of the turn [46, 49]. As a result, two tipping-out torques are added: a lean-induced tipping-out gravitational torque and a turn-induced tipping-out centrifugal torque [46, 49]. On a regular bicycle, these two torques act in opposite directions: the turn-induced tipping-out centrifugal torque is cancelled by a lean-induced tipping-in gravitational torque at the pelvis. Crucially, none of the participants was able to complete a simple obstacle course on the bricycle [46, 49]. This suggests that the non-negotiable tipping-out torque elicits proprioceptive feedback that makes the CNS think the rider is falling to the opposite side of the initiated turn. Because the CNS has learned to steer to the fall, completing the turn is not possible on the bricycle.

### *Two bicycle models*

Starting from the kinematic bicycle model in Fig. 3, I formulated two sets of EoM for the mechanical system, one nonlinear and one linear. The EoM for both bicycle models are derived in the Methods. The nonlinear EoM are obtained by combining the dynamics of the Acrobot and the double pendulum on a cart under bicycle-specific kinematic constraints [50]. This model is called the Steered Double Pendulum (SDP). The linear EoM are obtained from a linear 2-DoF benchmark model [47] by replacing the rear frame by a linearized double pendulum [50]. This linear model is called the Benchmark Double Pendulum (BDP).

Simulations using the nonlinear EoM of the SDP have the advantage that they mimic the fact that an internal model (linear in our simulations) typically is only an approximation of a nonlinear mechanical system. Simulations using linear EoM will not capture the inevitable differences in the dynamics of the internal and the mechanical model, and a good control performance may thus give an overly optimistic picture.

Simulations using the linear BDP have the advantage that this model captures steering torques that result from the passive (rider-independent) dynamics. Specifically, the model's passive dynamics involves steering torques that depend on the angular position  $\theta_1$  (sign and amplitude). These passive steering torques are necessary for the self-stability of the bicycle [47] and they also result in a much more relaxed steering behavior. The SDP does not have these passive steering torques and therefore has a much twitchier steering behavior, not representative of commercial bicycles. In the BDP but not in the SDP, the rider can in principle feel the angular position through the steering torque, but this potential feedback has been removed from  $C_{sens}$  and  $C_{comp}$  by pre-multiplying these matrices with  $[0 \quad -1 \quad 1]$ ; the 0 in the first position corresponds to the steering axis.

*A bicycle can be balanced using exafferent pelvic joint acceleration feedback*

I followed the same approach as in the simulations of standing balance control, but now the challenge is much more difficult: I try to control a 3-DoF underactuated (instead of a 1-DoF fully actuated) mechanical model using exafferent acceleration feedback from a single joint. As for standing balance control, I assume that the combined effects of motor and fusimotor noise on the sensory feedback roughly matches the effect pure sensor noise, and to implement this I use the noise variance of the sensory feedback (which depends on motor, fusimotor and pure sensor noise) as a common scale. The only difference is that the motor noise is two-dimensional, with a steering and a pelvic component. I assume that the two noise components are independent and have equal variance.

The evaluation of the simulation results is based on the same two requirements as for standing balance control: (1) the combined CoG lean angle RMSD must converge to zero with decreasing noise amplitude, and (2) the whole RMSD range that can be observed must also be produced by the model. There are physical constraints on the maximum RMSD that is possible. Although, in theory, a combined CoG at any position relative to the LoS can be brought above this LoS by means of steering, the maximum combined CoG lean angle for which this is possible in practice depends on the speed and the coefficient of friction. In [50], it is described (1) how the minimum turn radius can be calculated from speed and the coefficient of friction, and (2) how, for a given bicycle geometry, the corresponding critical steering angle can be calculated. For the speed and the bicycle geometry used in the simulations, this critical steering angle is 18.91 degrees.

The weights of the optimality criterium in Eq. 1 are calculated in the same way as for standing balance control but now using maxima for the lean and the steering angle, the pelvic and the steering torque. Compared to standing balance control, torque limits are much less important in bicycle balance control. This is because (1) turning the handlebars requires very little torque, and (2) for rotating the upper body there are strong axial muscles, producing

a large pelvic torque. As a maximum, I took the torque that is required to keep the upper body in a horizontal position on a Roman chair (a bed with an unsuspended upper body), but this maximum was never reached in the simulations.

The simulations demonstrated that, both for the linear BDP and the nonlinear SDP, the combined CoG lean angle RMSD converged to zero with decreasing noise amplitude. However, compared to the SDP, the BDP could produce much larger RMSD values without diverging away from the upright position. This is consistent with the much twitchier steering behavior of the SDP, making it harder to control.

Sample results for the BDP are shown in Fig. 4. Panel A shows that the highest value for the combined CoG lean angle RMSD is 2.77 from where it converges to 0 with decreasing noise amplitude. The maximum steering angle observed over the one-minute simulation period increased with noise amplitude, but the critical steering angle of 18.91 degrees was never reached.

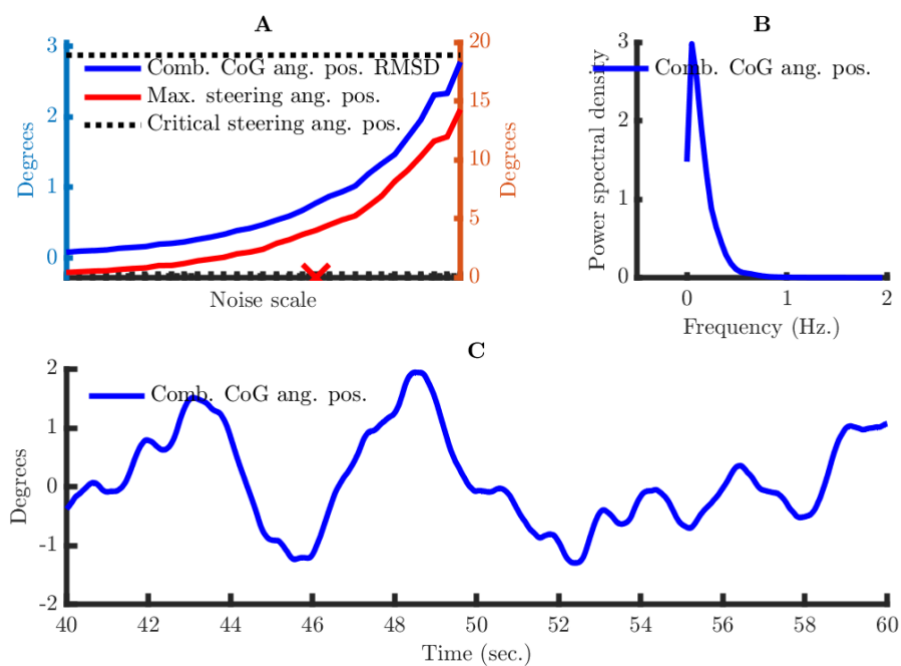


**Fig. 4: Simulation results for BDP bicycle balance control using exafferent acceleration feedback.** (A) Combined angular position (lean angle) RMSD (in blue), maximum steering angle in a one-minute period (in red), and critical

steering angle (in black). (B) Power spectral density of the combined CoG angular position for the noise scale that is indicated by a red V in panel A. (C) Example combined CoG angular position for the same noise scale as in B.

For completeness, in Fig. 5B and 5C, I added an example combined CoG angular position time course and its corresponding average psd. It is not informative to compare this time course to the angular position time courses when cycling on the public roads, because the latter task involves road boundaries, which requires control actions (steering) that are unrelated to balance control (i.e., staying between the road boundaries).

Concluding, exafferent pelvic joint acceleration feedback is sufficient to balance a bicycle and, for the BDP, it does so for a large part of the range of RMSD values that is theoretically possible. A bicycle can thus be balanced using the same type of feedback as for standing balance control: exafferent joint acceleration over the same axis as the angular position that is to be controlled.

## Discussion

### Summary of the results

For all motor tasks with an approximately linear mechanical system, optimal control actions are a simple linear combination of full state sensory feedback. When the sensory organs only provide incomplete feedback, such an approximately linear system allows for an extremely versatile type of control that is based on a CNS-internal dynamical system that estimates the states. This system can be implemented as a RNN and it uses a sensory model to update the state estimates using incomplete feedback. This computational system is fully specified by an optimality criterion for control performance, a forward model of the mechanical system, and a sensory model of the sensory feedback. This formalism is highly relevant for spindle primary afferents, which produce incomplete feedback. Specifically, the firing rates of spindle primary afferents scale with the exafferent joint acceleration that is produced by the non-muscular forces gravity, elasticity, and damping. Crucially, there exists a sensory model for this exafferent joint acceleration feedback that expresses it as a linear combination of the state variables. The resulting control mechanism simulates standing and bicycle balance control using realistic parameter values and with forcing torques that are feasible for humans.

### Contribution to the modelling of balance control

Several papers in the balance control literature have used an internal dynamical system to model the CNS within the framework of OFC [51-56]. It has been used for testing hypotheses about (1) the information in the sensory feedback (position, velocity, and/or acceleration) that is used for updating the state estimate [51, 52], (2) a mechanism that compensates for the sensorimotor delay [54], (3) intermittent versus continuous standing balance control [53], (4) non-linear components in the corrective responses to balance-perturbing stimuli [55], and (5) the control objective of the CNS (stabilization versus sway minimization) [56]. The main difference with this

paper is that I use OFC to test a hypothesis that is derived from sensory neurophysiology: Is exafferent joint acceleration feedback sufficient for balance control? Existing papers mainly demonstrate the scope of OFC in explaining different phenomena [51-56], and this paper demonstrates that it continues to be successful if the sensory feedback is constrained by the response properties of the relevant sensory organs. Of course, I do not want to suggest that spindle afferents only generate exafferent acceleration feedback; my only claim is that some spindle afferents do, and that this type of feedback is sufficient for the CNS to estimate position and velocity.

### **Short-range muscle stiffness and the mechanics of muscle spindles**

Because mechanical systems are second order (i.e., the highest derivative in the EoM is 2), acceleration has a well-defined relation with the state variables. However, there is no guarantee that the mechanics of the muscle spindles have the same structure as the mechanics of the limb to which these spindles belong. In fact, there is good evidence for short-range muscle stiffness and this potentially complicates the relation between the state variables and the spindle afferent firing rates [31, 57-59]. To deal with short-range muscle stiffness, [31] proposed that spindle output scales with a linear combination of the tension force and its first time derivative (yank). However, this same study also demonstrated that, in passive muscles, peak yank and peak acceleration predicted similar amounts of variance in the initial burst amplitudes [31]. Short-range muscle stiffness is thus consistent with spindle output at stretch onset that scales with peak acceleration. This was also demonstrated by a recent combined biomechanical-neurophysiological model of the muscle spindle that models short-range muscle stiffness at the level of cross-bridge kinetics [60].

### **Paradoxical muscle shortening**

Exafferent joint acceleration feedback effectively deals with the potential problems caused by paradoxical muscle shortening [61-63]. Paradoxical muscle shortening is due to compliance of the Achilles tendon, which makes

the body unstable, and necessitates muscle activity to maintain balance. Generating sufficient muscular tension results in paradoxical changes in muscle length: when the body rotates forward ( $\dot{\theta} > 0$ ), the calf muscles are actively shortened (producing a negative torque  $\tau < 0$ ) to maintain balance. As a result of this paradoxical muscle shortening, muscle length is negatively correlated with angular position [64]. If muscle spindle afferent firing rates would be proportional to muscle length, paradoxical muscle shortening would result in firing rate patterns that are opposite to those of a passive joint that is moved by an external torque. It is unclear how the CNS could interpret such a signal, and this was also noted by [64]. However, if the muscle spindle output reflects the exafferent joint acceleration component, the computational system can rely on a well-defined sensory internal model to successfully update the internal state estimate, as demonstrated in this paper.

At this point, it is important to discuss the sensory consequences of tendon compliance: the larger the compliance, the less the joint angular acceleration will reflect the extrafusal fiber acceleration. This would reduce the information in the spindle output (which depends on the extrafusal fiber acceleration) about the joint's state (which is constrained by joint angular acceleration via Eq. 3). A principled way to deal with a possible inaccurate information about the joint's state is by means of a dynamical system for the muscle-tendon unit in which the muscle and the tendons have their own dynamics. Dynamical systems have been used before to model the properties of sensory organs [53-55, 65, 66]. Such a dynamical system would become part of an extended mechanical system with additional output variables: lengths, velocities, and accelerations of the individual muscles (extrafusal fibers), both agonists and antagonists, and their corresponding tendons. The extrafusal fiber accelerations then co-determine (together with the fusimotor output to the intrafusal fibers) the muscle spindle firing rates. Note that, if the mechanical system is extended by a component for the muscle-tendon dynamics, also the computational system is extended by an internal model for this component.

### **Central mechanisms for cancelling re-afferent feedback**

Purely exafferent muscle spindle feedback requires perfectly coordinated fusimotor and skeletomotor control. It is difficult to argue that this is always the case, especially because the computational system must learn to compute fusimotor output that cancels the reafferent feedback. Thus, due to imperfectly coordinated fusimotor and skeletomotor control, the feedback may still contain a reafferent part. Central mechanisms exist via which reafferent feedback can be cancelled [67, 68] and they depend on a corollary discharge, an efference copy with a special role in the processing of sensory feedback. Similar mechanisms might also be used to cancel the reafferent acceleration component that could not be cancelled by fusimotor control.

### **More complex mechanical systems**

My model for balance control is general in the sense that it only depends on the mechanical system's EoM and some parameters for which realistic values can be found (see Methods). However, because the mechanical system may be complex, it may be difficult to obtain its EoM. Therefore, in this paper, I considered a restricted form of cycling in which the rider keeps his legs still, does not use them to carry weight, and relies on a motor for propulsion. Under these restrictions, I could derive EoM for the rider-bicycle combination. However, most cyclists transfer a large part of their weight to the pedals and the handlebars; downhill mountain bikers (the balance artists in the cycling community) even do this for the full 100 percent. To model bicycle balance control with less constraints on the rider's movements, we need EoM for a more general mechanical system in which (1) the lower body is no longer a part of the rear frame, and (2) the AoS for the combined upper and lower body is formed by saddle, pedals, and handlebars. For the rest of the model (sensory, computational, and motor output system), no new ingredients are needed.

**Conclusion**

This paper integrates theoretical views from motor control with experimental results from sensory neurophysiology and applies the resulting model to balance control. The result is a dynamical system that estimates the full state from the exafferent joint acceleration feedback generated by spindle primary afferents. The estimates obtained from this incomplete feedback is sufficient to control the balance of a standing body and a rider-bicycle combination.

## Methods

### Matlab toolbox

All simulations were performed using the Matlab Balance Control (BalCon) toolbox that is shared in the supplementary information, together with the scripts that produced the simulation results, including the figures. For every mechanical system, the BalCon toolbox contains one function that computes the EoM and their linearization. Most of the toolbox's functions are generic, in the sense that they can be used for all mechanical systems.

### Simulations of standing balance control

The computer simulations are based on difference equations that are discrete time versions of the differential equations that were presented in the Results section. The difference equations for the linear dynamical system under consideration are the following:

$$\begin{aligned}\mathbf{x}_{k+1} &= A_{dt}\mathbf{x}_k + B_{dt}u_k + B_{dt}m_k \\ y_k &= C_{Comp}\mathbf{x}_k + B_{dt}^{lo}m_k - B_{dt}^{lo}f_k + s_k\end{aligned}$$

In this equation,  $k$  indexes discrete time steps that are separated by a time interval  $dt$ . The matrices  $A_{dt}$  and  $B_{dt}$  are obtained from the well-known solution of a linear differential equation:  $A_{dt} = e^{A dt}$  and  $B_{dt} = A^{-1}(A_{dt} - I)B$ , in which  $I$  is the identity matrix [69]. The lower half of  $B_{dt}$  is denoted by  $B_{dt}^{lo}$ . The use of  $B_{dt}^{lo}$  instead of the inverse mass moment of inertia  $M^{-1}$  is explained in *A general mechanical model constrains the relation between acceleration, force input, and state variables*.

Optimal control is provided by the discrete time version of Eq. 7:

$$\hat{\mathbf{x}}_{k+1} = (A_{dt} - B_{dt}K_{dt})\hat{\mathbf{x}}_k + L_{dt}[y_k - C_{Comp}(A_{dt} - B_{dt}\hat{\mathbf{x}}_k)]$$

The mechanical system (the CIP) is specified by realistic and/or empirical values for its parameters: body length  $l = 1,85$  m., body mass  $m = 85$  kg., gravitational constant  $g = 9,8066$ , ankle stiffness  $k_{stiff} = 493.4706$  Nm/rad.

(64% of the critical stiffness), and ankle damping  $c_{damp} = 30 \text{ Nm}/(\text{rad./s})$  [38]. These parameter values also specify the linear approximation in Eq. 6. The CIP dynamics are simulated by the Matlab function ode45, which is based on an explicit Runge-Kutta (4,5) formula [70]. As depicted in Fig. 1, the input to the mechanical system is  $z_k = u_k + m_k$ , with  $u_k = -K_{dt}\hat{\mathbf{x}}_k$ , and the output is  $[\mathbf{x}_{k+1}^t, \ddot{\theta}_{k+1}]^t$ .

The feedback loop is closed by the sensory system that maps the output of the mechanical system ( $\ddot{\theta}_{k+1}$ ), the output of the fusimotor system ( $w_{k+1}$ ), and the pure sensory noise ( $s_{k+1}$ ) to the sensory feedback  $y_{k+1}$ :

$$y_{k+1} = C_{Sens} \begin{bmatrix} \ddot{\theta}_{k+1} \\ w_{k+1} \end{bmatrix} + s_{k+1}$$

To simulate CIP dynamics under closed-loop feedback control, one must add noise. I set the noise parameters such that the effects of motor and pure sensor noise on the sensory feedback are equal. As a common scale for the effects of these three noise types, I use the noise variance of the sensory feedback  $y_k$ : if the noise source is only sensory, then  $\text{var}(y_k) = \text{var}(s_k)$ , and if the noise source is only motor, then

$$\text{var}(y_k) = B_{dt}^{lo} \text{var}(m_k) B_{dt}^{lo^t} + C_{Comp} B_{dt} \text{var}(m_k) B_{dt}^t C_{Comp}^t \quad \text{Eq. 8}$$

In the simulations, I start from a noise scaling variable  $\sigma$  and (1) set  $\text{var}(s_k) = \sigma$ , (2) scale  $\text{var}(m_k)$  such that the expression on the right side of Eq. 8 equals  $\sigma$ , and (3) set  $\text{var}(f_k) = \text{var}(m_k)$ . I set the covariance  $\text{cov}(m_k, f_k)$  such that the shared variance of  $m_k$  and  $f_k$  is 50%.

The variance of the noise terms  $B_{dt} m_k$  (for the state equation, but also fed into the output equation) and  $-B_{dt}^{lo} f_k + s_k$  (for the output equation only) and their covariance are used as weights in the calculation of the Kalman gain  $L_{dt}$ . This Kalman gain is a part of the computational system, and we thus implicitly assume that the CNS learns the sensor and the motor noise amplitudes from experience.

To be realistic, the ankle torque in the simulations must be less than the maximum voluntary contraction (MVC) of the ankle muscles. Therefore, the output of the computational system is truncated at an empirically determined MVC. Because humans prefer a leaned forward position, I use plantarflexion MVC. In a study with 20 participants, the mean plantarflexion MVC was estimated to be 195 Nm [44].

In the simulations, I evaluate whether the CoG remains over the AoS, which is a fraction of the sole length. To determine the AoS, I use a body-to-sole-length ratio of 6.6 [71], place the ankle at 25% from the rear end of the sole, and assume that the CoG must remain at 10% from the front and the rear end of the sole. The latter assumption is required because there can be no reaction forces near the edge of the sole. This results in a critical angular position interval  $[-0.0758, 0.2293]$  rad. over the ankle joint.

The LQR gain  $K_{dt}$  depends on the weights of the optimality criterium in Eq. 1, the 2-by-2 matrix  $Q$  and the scalar  $R$ . These weights are set such that the precision ( $Q$ -dependent) and the energetic cost ( $R$ -dependent) component have an equal contribution to the optimality criterium. In this calculation, I set  $c = [0.0156 \quad 0]^t$  rad., in agreement with the observation that humans prefer a leaned forward position around 0.0156 rad. [72]. I use the maximum metric to calculate a diagonal matrix  $Q$  and a scalar  $R$  that produce equal values for  $x_{max}^t Q x_{max}$  and  $u_{max} R u_{max}$ . For the calculation of  $x_{max}$ , I start from the critical angular position interval  $[-0.0758, 0.2293]$  rad., and calculate the critical angular velocity from the maximum angle position frequency of 1.875 Hz reported in [45]. This results in  $x_{max} = [0.2137 \quad 0.3655]^t$ . I give angular position and angular velocity an equal contribution to the precision component by setting  $Q_{11}$  and  $Q_{22}$  such that  $0.2137^2 Q_{11} = 0.3655^2 Q_{22}$ . The critical torque  $u_{max} = 195$  is obtained from [44].

### A general mechanical model constrains the relation between acceleration, force input, and state variables

I now demonstrate the relation between  $C_{Sens}$  and  $C_{Comp}$  for a general multibody mechanical system (i.e., extending Eq. 5 to a multibody system). I use this more general relation to model bicycle balance control using exafferent joint acceleration feedback from the rider's upper body. I start from the following differential equation for a multibody mechanical system:

$$M(\boldsymbol{\theta})\ddot{\boldsymbol{\theta}} + D(\boldsymbol{\theta}, \dot{\boldsymbol{\theta}}) = H\mathbf{z} \quad \text{Eq. 9}$$

The vectors  $\boldsymbol{\theta}$ ,  $\dot{\boldsymbol{\theta}}$ ,  $\ddot{\boldsymbol{\theta}}$  and  $\mathbf{z}$  are, respectively, the positions, velocities, accelerations and forcing torques of a multibody mechanical system. Because not all joints have to be actuated (see the bicycle model for an example), I use the binary matrix  $H$  to distribute the forcing torques over the joints; rows of  $H$  that correspond to non-actuated joints are zero. The matrix  $M(\boldsymbol{\theta})$  is the mass moment of inertia and the vector  $D(\boldsymbol{\theta}, \dot{\boldsymbol{\theta}})$  captures all forces of the non-actuated system (gravity, centrifugal, damping, stiffness). In the CIP, the mass moment of inertia  $M(\boldsymbol{\theta})$  is independent of  $\boldsymbol{\theta}$  and was denoted by  $M$ . Note that Eq. 9 is more general than the familiar manipulator equation form [12], which splits  $D(\boldsymbol{\theta}, \dot{\boldsymbol{\theta}})$  into two terms of which one depends on gravity only.

Eq. 8 can be rewritten as follows:

$$\ddot{\boldsymbol{\theta}} - M(\boldsymbol{\theta})^{-1}H\mathbf{z} = -M(\boldsymbol{\theta})^{-1}D(\boldsymbol{\theta}, \dot{\boldsymbol{\theta}}) \quad \text{Eq. 10}$$

I now linearize the left side of Eq. 10 with respect to  $\ddot{\boldsymbol{\theta}}$  and  $\boldsymbol{\tau}$ , and the right side with respect to  $\boldsymbol{\theta}$  and  $\dot{\boldsymbol{\theta}}$ . Next, I evaluate the Jacobian of this linearization at the unstable fixed point  $[\boldsymbol{\theta}; \dot{\boldsymbol{\theta}}] = [\mathbf{0}; \mathbf{0}]$ . The Jacobian of the left side is  $[I, -M(\mathbf{0})^{-1}H]$ , in which  $I$  is the identity matrix. The Jacobian of the right side requires symbolic differentiation, and the outcome of this operation is denoted by  $J_{[\boldsymbol{\theta}; \dot{\boldsymbol{\theta}}]}(\mathbf{0}; \mathbf{0})$ . Inserting the linear approximations in the left- and the right side of Eq. 10, one obtains

$$[I, -M(\mathbf{0})^{-1}H] \begin{bmatrix} \ddot{\boldsymbol{\theta}} \\ \mathbf{z} \end{bmatrix} \approx J_{[\boldsymbol{\theta}; \dot{\boldsymbol{\theta}}]}(\mathbf{0}; \mathbf{0}) \begin{bmatrix} \boldsymbol{\theta} \\ \dot{\boldsymbol{\theta}} \end{bmatrix} \quad \text{Eq. 11}$$

The sensory feedback mapping matrices  $C_{Sens}$  and  $C_{Comp}$  are equal to the Jacobians in, respectively, the left- and the right side of Eq. 11. We thus obtain

$$C_{Sens} \begin{bmatrix} \ddot{\theta} \\ \mathbf{z} \end{bmatrix} \approx C_{Comp} \begin{bmatrix} \theta \\ \dot{\theta} \end{bmatrix}$$

Every row in  $C_{Sens}$  specifies the difference between the acceleration at a single joint and a linear combination of the forcing torques. The corresponding row in  $C_{Comp}$  specifies a linear combination of the state variables.

Note that these Jacobians also appear in the linearization of the EoM:

$$\ddot{\theta} = -M(\theta)^{-1}D(\theta, \dot{\theta}) + M(\theta)^{-1}H\tau$$

$$\ddot{\theta} \approx J_{[\theta; \dot{\theta}]}(\mathbf{0}; \mathbf{0}) \begin{bmatrix} \theta \\ \dot{\theta} \end{bmatrix} + M(\mathbf{0})^{-1}H\tau$$

Thus, the EoM in state-space form,  $\begin{bmatrix} \dot{\theta} \\ \ddot{\theta} \end{bmatrix} = \dot{\mathbf{x}} = A\mathbf{x} + B\tau$ , have coefficient matrices  $A$  and  $B$ , of which the lower halves are equal to, respectively,  $J_{[\theta; \dot{\theta}]}(\mathbf{0}; \mathbf{0})$  and  $M(\mathbf{0})^{-1}H$ . In the Methods section, these lower halves are denoted by  $A^{lo}$  and  $B^{lo}$ .

### The SDP EoM

The SDP EoM can be assembled from three components: (1) the EoM of a double compound pendulum with an actuated base (like the double compound pendulum on a cart, DCPC) and an actuated pelvic joint (like the Acrobot), (2) a planar kinematic bicycle model [73] that produces a formula for the acceleration at this base, and (3) a torsional spring-mass-damper system for the steering angle. Specifically, I model the angular positions  $\theta_1$  and  $\theta_2$  as the result of a double compound pendulum on a (zero-mass) cart (DCPC) and acceleration equal to  $\alpha(\delta)$ , the centrifugal acceleration derived under the planar kinematic bicycle model (see further). The EoM for this DCPC can be written as follows:

$$\begin{aligned}
& \begin{bmatrix} d_1 \cos(\theta_1) \\ d_2 \cos(\theta_2) \end{bmatrix} \alpha(\delta) + \begin{bmatrix} d_3 & d_4 \cos(\theta_1 - \theta_2) \\ d_4 \cos(\theta_1 - \theta_2) & d_5 \end{bmatrix} \begin{bmatrix} \ddot{\theta}_1 \\ \ddot{\theta}_2 \end{bmatrix} \\
& + \begin{bmatrix} 0 & d_4 \sin(\theta_1 - \theta_2) \theta_2 \\ d_4 \sin(\theta_1 - \theta_2) \phi_1 & 0 \end{bmatrix} \begin{bmatrix} \dot{\theta}_1 \\ \dot{\theta}_2 \end{bmatrix} \\
& + \begin{bmatrix} -f_1 \sin(\theta_1) \\ -f_2 \sin(\theta_2) \end{bmatrix} \\
& + \begin{bmatrix} k_{pelvis}(\theta_1 - \theta_2) + c_{pelvis}(\dot{\theta}_1 - \dot{\theta}_2) \\ -k_{pelvis}(\theta_1 - \theta_2) - c_{pelvis}(\dot{\theta}_1 - \dot{\theta}_2) \end{bmatrix} = \begin{bmatrix} 0 \\ T_\theta \end{bmatrix}
\end{aligned} \quad \text{Eq. 12}$$

These EoM are obtained by first applying the Euler-Lagrange method to the DCPC with a zero-mass cart, and then adding the constraint that the cart is controlled by the steering-induced centrifugal acceleration  $\alpha(\delta)$ . The derivation of the DCPC EoM using the Euler-Lagrange method can be found in the literature. Here, I started from Bogdanov (74) and added stiffness (with constant  $k_{pelvis}$ ), damping (with constant  $c_{pelvis}$ ) and torque input  $T_\theta$  at the pelvic joint (between the upper and the lower body), similar to the Acrobot [12]. Next, I added the constraint that the angles  $\theta_1$  and  $\theta_2$  have no direct effect on the position of the base of the first rod (in the DCPC, the point where the cart is attached). This constraint follows from the fact that the bicycle's wheels are oriented perpendicular to the cart's wheels. Under this constraint, the position of the base of the first rod is fully controlled by the steering-induced centrifugal acceleration  $\alpha(\delta)$ .

The constants in Eq. 12 are defined as follows:

$$\begin{aligned}
d_1 &= m_1 l_1 + m_2 L_1 \\
d_2 &= m_2 l_2 \\
d_3 &= m_1 l_1^2 + m_2 L_1^2 + I_1 \\
d_4 &= m_2 L_1 l_2 \\
d_5 &= m_2 l_2^2 + I_2 \\
f_1 &= (m_1 l_1 + m_2 L_1) g \\
f_2 &= m_2 l_2 g
\end{aligned} \quad \text{Eq. 13}$$

The constants  $m_1$ ,  $L_1$ ,  $l_1$  and  $I_1$  are, respectively, the mass, the length, the CoG ( $L_1/2$ ) and the mass moment of inertia of the double pendulum's first rod, which represents the bicycle and the rider's lower body. The constants  $m_2$ ,

$L_2$ ,  $l_2$  and  $I_2$  are defined in the same way, but now for the second rod, which represents the rider's upper body. Finally,  $g$  is the gravitational constant.

I now give the formula for the centrifugal acceleration  $\alpha(\delta)$  that can be derived from a well-known planar bicycle model from the vehicle dynamics literature [73]:

$$\alpha(\delta) = v^2 \frac{\cos(\beta(\delta))}{W} \tan(\delta)$$

This formula depends on the speed  $v$ , the bicycle wheelbase  $W$ , and the so-called slip angle  $\beta(\delta)$ , which is the angle between the velocity vector of the combined CoG and the LoS. This slip angle can be obtained as follows:

$$\beta(\delta) = \tan^{-1} \left( \frac{w_r \tan(\delta)}{W} \right)$$

In this equation,  $w_r$  is the position of the combined CoG on the LoS. More precisely,  $w_r$  is the distance between the road contact point of the rear wheel and the orthogonal projection of the combined CoG on the LoS. For realistic values ( $W = 1.02$ ,  $w_r = 0.3$ ,  $-20^\circ < \delta < 20^\circ$ ), the slip angle  $\beta(\delta)$  is almost a linear function of  $\delta$ :

$$\beta(\delta) \approx \frac{w_r \delta}{W}$$

For steering angles  $-20^\circ < \delta < 20^\circ$ , all deviations from linearity are less than 0.36%. In my simulations, I have used this approximation.

Finally, I introduce the model for the steering angle  $\delta$ . This model assumes that the steering angle is fully controlled by rider-applied forces on the handlebars; I thus ignore all forces that may contribute to a bicycle's self-stability. The steering assembly consists of the front wheel, the fork, the handlebars, and the rider's arms. I model this assembly as a torsional spring-mass-damper system:

$$M_{steer} \ddot{\delta} + c_{steer} \dot{\delta} + k_{steer} \delta = T_\delta \quad \text{Eq. 14}$$

In this equation,  $M_{steer}$  is the assembly's mass moment of inertia,  $c_{steer}$  its damping, and  $k_{steer}$  its stiffness. The input to the steering assembly is the net torque produced by the rider's arm muscles and denoted by  $T_\delta$ .

It is possible to derive expressions for the second derivatives  $\ddot{\delta}$  and  $[\ddot{\theta}_1, \ddot{\theta}_2]^T$  from Eq. 12 and Eq. 14. These expressions are complicated and not insightful. In my simulations, I use these expressions to define the state-space equations  $\dot{\mathbf{x}} = \Omega(\mathbf{x}, \mathbf{u} + \mathbf{m})$  for the state variables  $\mathbf{x} = [\delta, \theta_1, \theta_2, \dot{\delta}, \dot{\theta}_1, \dot{\theta}_2]^T$ , external torques  $\mathbf{u} = [T_\delta, T_\theta]^T$ , and motor noise  $\mathbf{m}$ .

### The BDP EoM

The BDP is based on three ideas. The first idea is to follow the approach of [47] and derive linearized EoM for a bicycle with the rider's lower body rigidly attached to the rear frame and no upper body. These linearized EoM depend on a number of constants, and I chose these constants such that (1) the front frame is as similar as possible to the self-stable benchmark bicycle model described by [47], and (2) the lengths and masses are as similar as possible to the SDP. The second idea is to model the interactions between the upper body and the rear frame (which includes the lower body) by the linearized EoM of the double compound pendulum, similar to [75]. Finally, the third idea is to first derive the BDP EoM without stiffness and damping terms, and to add these terms only in the last step.

The approach of [47] involves a method to calculate the defining matrices of linearized EoM of the following type:

$$\mathbf{M} \begin{bmatrix} \ddot{\delta} \\ \ddot{\theta}_1 \\ \ddot{\theta}_2 \end{bmatrix} + \mathbf{C} \begin{bmatrix} \dot{\delta} \\ \dot{\theta}_1 \\ \dot{\theta}_2 \end{bmatrix} + \mathbf{K} \begin{bmatrix} \delta \\ \theta_1 \\ \theta_2 \end{bmatrix} = 0$$

The matrices  $\mathbf{M}$ ,  $\mathbf{C}$  and  $\mathbf{K}$  are functions of several constants (angles, lengths, masses, mass moments of inertia, gravitational acceleration, speed) that characterize the bicycle components and the internal forces that act on them. (I used the same symbols as [47], and therefore  $\mathbf{M}$  has a different meaning as in the previous sections.) [47] only derived linearized EoM for bicycles with a rider that was rigidly attached to the rear frame. Thus, the upper body angular position  $\theta_2$  is absent from their EoM. This missing component can be obtained by linearizing the double pendulum EoM which models the

interactions between  $\theta_1$  and  $\theta_2$ . Schematically, each of the matrices  $\mathbf{M}$ ,  $\mathbf{C}$  and  $\mathbf{K}$  is composed as follows:

$$\begin{bmatrix} \text{MP}(1,1) & \text{MP}(1,2) & 0 \\ \text{MP}(2,1) & \text{MP}(2,2) & 0 \\ 0 & 0 & 0 \end{bmatrix} + \begin{bmatrix} 0 & 0 & 0 \\ 0 & \text{DP}(1,1) & \text{DP}(1,2) \\ 0 & \text{DP}(2,1) & \text{DP}(2,2) \end{bmatrix}$$

in which “MP” denotes “Meijaard, Papadopoulos et al” [47], and “DP” denotes “Double Pendulum”. The MP calculations were performed by means of the Matlab toolbox Jbike6 [76], in which I entered the constants for a bicycle with the rider’s lower body rigidly attached to the rear frame and no upper body. This produced the constants  $\text{MP}(i,j)$  ( $i,j = 1,2$ ) for  $\mathbf{M}$ ,  $\mathbf{C}$  and  $\mathbf{K}$ .

I now model the interactions between the upper body and the rear frame by the linearized EoM of the double compound pendulum. The nonlinear EoM of the double compound pendulum are obtained from Eq. 12 by removing the terms that correspond to the centrifugal acceleration  $\alpha(\delta)$ , the stiffness and the damping:

$$\begin{aligned} & \begin{bmatrix} d_3 & d_4 \cos(\theta_1 - \theta_2) \\ d_4 \cos(\theta_1 - \theta_2) & d_5 \end{bmatrix} \begin{bmatrix} \ddot{\theta}_1 \\ \ddot{\theta}_2 \end{bmatrix} \\ & + \begin{bmatrix} 0 & d_4 \sin(\theta_1 - \theta_2) \theta_2 \\ d_4 \sin(\theta_1 - \theta_2) \theta_1 & 0 \end{bmatrix} \begin{bmatrix} \dot{\theta}_1 \\ \dot{\theta}_2 \end{bmatrix} + \begin{bmatrix} -f_1 \sin(\theta_1) \\ -f_2 \sin(\theta_2) \end{bmatrix} \\ & = \begin{bmatrix} 0 \\ T_\theta \end{bmatrix} \end{aligned}$$

I evaluate these EoM at  $\theta_1 = \theta_2$  and replace  $\sin(x)$  by its linear approximation near 0:  $\sin(x) \approx x$ . This results in

$$\begin{bmatrix} d_3 & d_4 \\ d_4 & d_5 \end{bmatrix} \begin{bmatrix} \ddot{\theta}_1 \\ \ddot{\theta}_2 \end{bmatrix} + \begin{bmatrix} -f_1 & 0 \\ 0 & -f_2 \end{bmatrix} \begin{bmatrix} \theta_1 \\ \theta_2 \end{bmatrix} = \begin{bmatrix} 0 \\ T_\theta \end{bmatrix}$$

The constants  $d_3$ ,  $d_4$  and  $d_5$  contain elements that must be added to the matrix  $\mathbf{M}$ , and the constants  $f_1$  and  $f_2$  contain elements that must be added to the matrix  $\mathbf{K}$  (for the definitions, see Eq. 13). I will use the notation  $\text{DP}(i,j)$  ( $i,j = 1,2$ ) to denote these elements. For  $\mathbf{M}$ , the following elements are added:

- $\text{DP}(1,1) = m_2 L_1^2$
- $\text{DP}(1,2) = \text{DP}(2,1) = d_4 = m_2 L_1 l_2$
- $\text{DP}(2,2) = d_5 = m_2 l_2^2 + I_2$

And for  $\mathbf{K}$ , the following elements are added:

- $DP(1,1) = m_2 L_1 g$
- $DP(2,2) = -f_2 = -m_2 l_2 g$

Finally, I added stiffness and damping terms that were also added to the SDP. The stiffness and damping terms were added to, respectively,  $\mathbf{K}$  and  $\mathbf{C}$ .

### **Stiffness and damping parameters for the SDP and the BDP**

Compared to the ankle joint, much less is known about the stiffness and damping of the steering and pelvic joint. These are not joints in the strict biomechanical sense because they involve more than the interface between two bones; the steering joint involves both the arms and part of the upper body, and the pelvic joint involves both the hip joint (head of femur and acetabulum) and the lumbosacral joint (lumbar spine and sacrum). For the steering joint, I calculated the stiffness from an empirically determined time constant, as described in [50]. And for the pelvic joint, I chose a stiffness coefficient such that the elastic force was 10 percent of the average (over upper and lower body) gravitational force; this allowed the upper and the lower body to fall with different accelerations. The damping ratio for both joints was set at 20, which is a strongly overdamped system. Strong damping was necessary for simulating the SDP; a critical damping ratio of 1 (the minimum damping that is required to suppress the spring-induced oscillations) resulted in numerical inaccuracies in the ODE solver (Matlab's ode45) even at very low noise levels. The BDP could be simulated for a wide range of damping ratio's, including critical damping.

## References

1. Åström KJ. Introduction to stochastic control theory: Courier Corporation; 2012.
2. Forbes PA, Chen A, Blouin J-S. Sensorimotor control of standing balance. *Handbook of clinical neurology*. 2018;159:61-83.
3. Proske U, Gandevia SC. The proprioceptive senses: their roles in signaling body shape, body position and movement, and muscle force. *Physiological reviews*. 2012.
4. Fitzpatrick R, Rogers DK, McCloskey D. Stable human standing with lower-limb muscle afferents providing the only sensory input. *The Journal of physiology*. 1994;480(2):395-403.
5. Mergner T, Schweigart G, Fennell L, Maurer C. Posture Control in Vestibular-Loss Patients. *Annals of the New York Academy of Sciences*. 2009;1164(1):206-15.
6. Young AS, Rosengren SM, Welgampola MS. Disorders of the inner-ear balance organs and their pathways. *Handbook of Clinical Neurology*. 2018;159:385-401.
7. Macefield VG, Knellwolf TP. Functional properties of human muscle spindles. *Journal of neurophysiology*. 2018;120(2):452-67.
8. Dimitriou M. Human muscle spindles are wired to function as controllable signal-processing devices. *Elife*. 2022;11:e78091.
9. Banks RW, Ellaway PH, Prochazka A, Proske U. Secondary endings of muscle spindles: Structure, reflex action, role in motor control and proprioception. *Experimental Physiology*. 2021;106(12):2339-66.
10. Kawato M. Internal models for motor control and trajectory planning. *Current opinion in neurobiology*. 1999;9(6):718-27.
11. Wolpert DM, Ghahramani Z, Jordan MI. An internal model for sensorimotor integration. *Science*. 1995;269(5232):1880-2.
12. Tedrake R. Underactuated Robotics: Algorithms for Walking, Running, Swimming, Flying, and Manipulation (Course Notes for MIT 6.832). Downloaded on 20-08-2021 from <http://underactuated.mit.edu/>. 2021.
13. Wolpert DM. Computational approaches to motor control. *Trends in cognitive sciences*. 1997;1(6):209-16.
14. Scott SH. Optimal feedback control and the neural basis of volitional motor control. *Nature Reviews Neuroscience*. 2004;5(7):532-45.
15. Todorov E. Optimality principles in sensorimotor control. *Nature neuroscience*. 2004;7(9):907-15.
16. Slijkhuis FS, Keemink SW, Lanillos P. Closed-form control with spike coding networks. *IEEE Transactions on Cognitive and Developmental Systems*. 2023.
17. Boerlin M, Machens CK, Denève S. Predictive coding of dynamical variables in balanced spiking networks. *PLoS computational biology*. 2013;9(11):e1003258.
18. Calaim N, Dehmelt FA, Gonçalves PJ, Machens CK. The geometry of robustness in spiking neural networks. *Elife*. 2022;11:e73276.
19. Körding KP, Wolpert DM. Bayesian decision theory in sensorimotor control. *Trends in cognitive sciences*. 2006;10(7):319-26.

20. Clemens IA, De Vrijer M, Selen LP, Van Gisbergen JA, Medendorp WP. Multisensory processing in spatial orientation: an inverse probabilistic approach. *Journal of Neuroscience*. 2011;31(14):5365-77.
21. Dimitriou M, Edin BB. Discharges in human muscle spindle afferents during a key-pressing task. *The Journal of physiology*. 2008;586(22):5455-70.
22. Peterka RJ. Sensory integration for human balance control. *Handbook of clinical neurology*. 2018;159:27-42.
23. Peterka RJ. Sensorimotor integration in human postural control. *Journal of neurophysiology*. 2002;88(3):1097-118.
24. Edin BB, Vallbo A. Muscle afferent responses to isometric contractions and relaxations in humans. *Journal of neurophysiology*. 1990;63(6):1307-13.
25. Vallbo A. Human muscle spindle discharge during isometric voluntary contractions. Amplitude relations between spindle frequency and torque. *Acta Physiologica Scandinavica*. 1974;90(2):319-36.
26. Burke D, Hagbarth K-E, Löfstedt L. Muscle spindle responses in man to changes in load during accurate position maintenance. *The Journal of Physiology*. 1978;276(1):159-64.
27. Burke D, Hagbarth K-E, Löfstedt L. Muscle spindle activity in man during shortening and lengthening contractions. *The Journal of physiology*. 1978;277(1):131-42.
28. Hulliger M, Nordh E, Vallbo A. The absence of position response in spindle afferent units from human finger muscles during accurate position holding. *The Journal of Physiology*. 1982;322(1):167-79.
29. Hulliger M, Nordh E, Vallbo A. Discharge in muscle spindle afferents related to direction of slow precision movements in man. *The Journal of Physiology*. 1985;362(1):437-53.
30. Edin BB, Vallbo A. Dynamic response of human muscle spindle afferents to stretch. *Journal of neurophysiology*. 1990;63(6):1297-306.
31. Blum KP, Lamotte D'Incamps B, Zytnicki D, Ting LH. Force encoding in muscle spindles during stretch of passive muscle. *PLoS computational biology*. 2017;13(9):e1005767.
32. Hagbarth K-E, Vallbo Å. Discharge characteristics of human muscle afferents during muscle stretch and contraction. *Experimental Neurology*. 1968;22(4):674-94.
33. Dimitriou M. Human muscle spindle sensitivity reflects the balance of activity between antagonistic muscles. *Journal of Neuroscience*. 2014;34(41):13644-55.
34. Dimitriou M, Edin BB. Human muscle spindles act as forward sensory models. *Current Biology*. 2010;20(19):1763-7.
35. Morasso PG, Sanguineti V. Ankle muscle stiffness alone cannot stabilize balance during quiet standing. *Journal of neurophysiology*. 2002;88(4):2157-62.
36. Morasso PG, Schieppati M. Can muscle stiffness alone stabilize upright standing? *Journal of neurophysiology*. 1999;82(3):1622-6.
37. Loram ID, Lakie M. Direct measurement of human ankle stiffness during quiet standing: the intrinsic mechanical stiffness is insufficient for stability. *The journal of physiology*. 2002;545(3):1041-53.
38. Casadio M, Morasso PG, Sanguineti V. Direct measurement of ankle stiffness during quiet standing: implications for control modelling and clinical application. *Gait & posture*. 2005;21(4):410-24.
39. Lockhart DB, Ting LH. Optimal sensorimotor transformations for balance. *Nature neuroscience*. 2007;10(10):1329-36.

40. Welch TD, Ting LH. A feedback model explains the differential scaling of human postural responses to perturbation acceleration and velocity. *Journal of neurophysiology*. 2009;101(6):3294-309.
41. Safavynia SA, Ting LH. Long-latency muscle activity reflects continuous, delayed sensorimotor feedback of task-level and not joint-level error. *Journal of neurophysiology*. 2013;110(6):1278-90.
42. Miall RC, Wolpert DM. Forward models for physiological motor control. *Neural networks*. 1996;9(8):1265-79.
43. Brunton SL, Kutz JN. *Data-driven science and engineering: Machine learning, dynamical systems, and control*: Cambridge University Press; 2019.
44. Vette AH, Masani K, Nakazawa K, Popovic MR. Neural-mechanical feedback control scheme generates physiological ankle torque fluctuation during quiet stance. *IEEE Transactions on Neural Systems and Rehabilitation Engineering*. 2010;18(1):86-95.
45. Soames R, Atha J. The spectral characteristics of postural sway behaviour. *European journal of applied physiology and occupational physiology*. 1982;49:169-77.
46. Dong O, Graham C, Grewal A, Parrucci C, Ruina A. The bricycle: a bicycle in zero gravity can be balanced or steered but not both. *Vehicle system dynamics*. 2014;52(12):1681-94.
47. Meijaard JP, Papadopoulos JM, Ruina A, Schwab AL. Linearized dynamics equations for the balance and steer of a bicycle: a benchmark and review. *Proceedings of the Royal Society of London A: Mathematical, Physical and Engineering Sciences*. 2007;463(2084):1955-82.
48. Kooijman J, Meijaard JP, Papadopoulos JM, Ruina A, Schwab A. A bicycle can be self-stable without gyroscopic or caster effects. *Science*. 2011;332(6027):339-42.
49. Dong O, Graham C, Grewal A, Parrucci C, Ruina A. A bicycle in zero gravity is unrideable (The bricycle) 2014 [updated 17-03-2014]. Available from: <https://youtu.be/rNQdSfgJDNM?si=RXDK-mXVMDGpXtch>.
50. Maris E. A bicycle can be balanced by stochastic optimal feedback control but only with accurate speed estimates. *PLoS one*. 2023;18(2):e0278961.
51. Kiemel T, Oie KS, Jeka JJ. Multisensory fusion and the stochastic structure of postural sway. *Biological cybernetics*. 2002;87(4):262-77.
52. Jeka J, Kiemel T, Creath R, Horak F, Peterka R. Controlling human upright posture: velocity information is more accurate than position or acceleration. *Journal of neurophysiology*. 2004;92(4):2368-79.
53. Van Der Kooij H, De Vlugt E. Postural responses evoked by platform perturbations are dominated by continuous feedback. *Journal of neurophysiology*. 2007;98(2):730-43.
54. van der Kooij H, Jacobs R, Koopman B, Grootenboer H. A multisensory integration model of human stance control. *Biological cybernetics*. 1999;80:299-308.
55. Van Der Kooij H, Peterka RJ. Non-linear stimulus-response behavior of the human stance control system is predicted by optimization of a system with sensory and motor noise. *Journal of computational neuroscience*. 2011;30:759-78.
56. Kiemel T, Zhang Y, Jeka JJ. Identification of neural feedback for upright stance in humans: stabilization rather than sway minimization. *Journal of Neuroscience*. 2011;31(42):15144-53.

57. Campbell K, Lakie M. A cross-bridge mechanism can explain the thixotropic short-range elastic component of relaxed frog skeletal muscle. *The Journal of physiology*. 1998;510(3):941-62.
58. Campbell KS, Moss RL. A thixotropic effect in contracting rabbit psoas muscle: prior movement reduces the initial tension response to stretch. *The Journal of Physiology*. 2000;525(2):531-48.
59. Campbell KS, Moss RL. History-dependent mechanical properties of permeabilized rat soleus muscle fibers. *Biophysical journal*. 2002;82(2):929-43.
60. Blum KP, Campbell KS, Horslen BC, Nardelli P, Housley SN, Cope TC, et al. Diverse and complex muscle spindle afferent firing properties emerge from multiscale muscle mechanics. *Elife*. 2020;9:e55177.
61. Loram ID, Maganaris CN, Lakie M. Paradoxical muscle movement in human standing. *The Journal of physiology*. 2004;556(3):683-9.
62. Loram ID, Maganaris CN, Lakie M. Active, non-spring-like muscle movements in human postural sway: how might paradoxical changes in muscle length be produced? *The Journal of physiology*. 2005;564(1):281-93.
63. Loram ID, Maganaris CN, Lakie M. Human postural sway results from frequent, ballistic bias impulses by soleus and gastrocnemius. *The Journal of physiology*. 2005;564(1):295-311.
64. Di Giulio I, Maganaris CN, Baltzopoulos V, Loram ID. The proprioceptive and agonist roles of gastrocnemius, soleus and tibialis anterior muscles in maintaining human upright posture. *The Journal of physiology*. 2009;587(10):2399-416.
65. Kuo AD. An optimal state estimation model of sensory integration in human postural balance. *Journal of neural engineering*. 2005;2(3):S235.
66. Laurens J, Angelaki DE. A unified internal model theory to resolve the paradox of active versus passive self-motion sensation. *Elife*. 2017;6:e28074.
67. Crapse TB, Sommer MA. Corollary discharge across the animal kingdom. *Nature Reviews Neuroscience*. 2008;9(8):587-600.
68. Poulet JF, Hedwig B. New insights into corollary discharges mediated by identified neural pathways. *Trends in neurosciences*. 2007;30(1):14-21.
69. DeCarlo RA. *Linear systems: A state variable approach with numerical implementation*: Prentice-Hall, Inc.; 1989.
70. Shampine LF, Reichelt MW. The matlab ode suite. *SIAM journal on scientific computing*. 1997;18(1):1-22.
71. Tremblay S. Height-to-Foot-Size Ratio [cited 2023 24-9]. Available from: <https://www.livestrong.com/article/491821-height-to-foot-size-ratio/>.
72. Rasman BG, Forbes PA, Peters RM, Ortiz O, Franks I, Inglis JT, et al. Learning to stand with unexpected sensorimotor delays. *Elife*. 2021;10:e65085.
73. Rajamani R. *Vehicle dynamics and control*: Springer Science & Business Media; 2011.
74. Bogdanov A. *Optimal control of a double inverted pendulum on a cart*. Oregon Health and Science University, Tech Rep CSE-04-006, OGI School of Science and Engineering, Beaverton, OR. 2004.
75. Dialynas G, Christoforidis C, Happee R, Schwab A. Rider control identification in cycling taking into account steering torque feedback and sensory delays. *Vehicle System Dynamics*. 2022:1-25.
76. A.L. Schwab JMP, A. Ruina and A. Dressel. JBike6, a benchmark for bicycle motion [cited 2022 14-7-2022]. Available from: [http://ruina.tam.cornell.edu/research/topics/bicycle\\_mechanics/JBike6\\_web\\_folde](http://ruina.tam.cornell.edu/research/topics/bicycle_mechanics/JBike6_web_folde)

